Laser amplification of incoherent radiation

Lionel N. Menegozzi
Department of Physics, University of Arizona, Tucson, Arizona 85721

Willis E. Lamb, Jr.
Department of Physics and Optical Sciences Center, University of Arizona, Tucson, Arizona 85721

(Received 2 June 1977)

The amplification of noise in a laser amplifier is treated theoretically. The model for the active medium and its description using density-matrix techniques, are taken from the theory of laser operation. The fundamental concern of this investigation is the spectral behavior of the radiation in the nonlinear regime; hence, the formalism is written from the onset in the frequency domain. The statistics of the light are gradually modified by the nonlinear amplification process, and expressions are derived for the rate of change of fluctuations in intensity as a measure of statistical changes. These expressions should be easily susceptible to detailed experimental observations. In addition, the range of validity of Litvak's Gaussian-statistics approximation is discussed with some detail. In the homogeneous-broadening case, the evolution of initially broadband Gaussian radiation toward quasimonochromatic oscillations with laserlike statistics is extensively explored in several numerical examples. The connections of this study with the time-domain work of Risken and Nummedal, on self-pulsing in a ring-laser configuration, are clearly established. Finally, spectral-narrowing and -rebroadening effects in Doppler-broadened media are discussed both analytically and with numerical examples. These examples show the distinct contribution of pulsations in the population ("Raman-type terms"), and saturation phenomena. The predicted narrowing-rebroadening rate is compared with expressions found in previous literature.

I. INTRODUCTION

Radio astronomy observations of anomalous maser radiation from interstellar medium, as well as the development of high-gain gas laser amplifiers, has renewed interest in the problem of nonlinear amplification of broadband noise. The amplified signals may be externally applied, or intrinsic to the active medium itself as in the case of amplified spontaneous emission.

There are numerous theoretical speculations about the cosmic maser radiation. However, to the best of our knowledge, satisfactory relations between the observed properties of such radiation and the source parameters have not been well established. In the case of high-power laser amplifiers, these may be intended to amplify a known coherent signal, but noise inevitably accompanies the output signal. In the linear regime, it is well known that the amplified noise is spectrally narrowed; but much less is known about the behavior of the field in the nonlinear regime. It seems to us that the main roadblock, in both cases, is that there is no satisfactory theory of the underlying amplification process. The present article is an attempt to provide the elements of such a theory.

The problem of coherent light such as a pulse propagating through a laser amplifier has been widely investigated by numerous authors.[1-4] Nevertheless, the propagation of incoherent light, white noise or blackbody radiation, does not follow in any direct way from these investigations because of saturation effects and combination tones. These effects not only contribute to change the spectrum but also change the statistical properties of the noise signal propagating through the amplifier.

In the past several years, a number of theoretical and experimental articles have been published dealing with several aspects of the problem at hand, e.g., amplified spontaneous emission, spectral narrowing and rebroadening, statistical properties of the radiation, possible self-pulsing, etc.[5-13] In our opinion, many of the theoretical contributions are inadequate because they are either based on semiphenomenological, oversimplified rate equations (a dangerous procedure when dealing with nonlinear phenomena); or they make use of unwarranted assumptions concerning the statistical behavior of the stochastic radiation during propagation. Others, finally, are restricted to the small signal regime. Therefore, we wish to provide a formalism based on first principles, and give a sound treatment of at least some definite problems of nonlinear radiative transfer.

In order to limit the scope of this investigation, the emphasis of this paper is on the well-defined problem of a laboratory laser amplifier, with noise as an input signal and one-way power flow. This problem already contains most of the important physical features, and indeed most of the complications associated with the nonlinear nature of the general problem. The model is a basic one, and limitations which are inherent to it can be dealt with in later stages. For example, in many labora-

tory amplifiers as well as in interstellar masers, the noise that is generated in the active medium itself is often a weak source[7,9]; however, spontaneous emission can be included by adding noise terms to the equations of radiative transport.[14,5] Next, the formalism developed here can be extended to allow for a two-way power flow, and diffraction effects which are of practical concern in a long amplifier.

The model for the active medium, and its description using density-matrix techniques are taken from laser theory.[15] Both the model and its description have been highly successful in many laser problems and the same should be so for the astrophysical problem, as well as for high-power laser amplifiers.

The paper is divided into five sections. In Sec. II we summarize the derivation of the field-medium coupled equations for a two-level atomic system under a steady-rate pumping mechanism. An important concern is the spectrum of the amplified radiation, and the formalism is written in the frequency domain. Section II also contains the definition of a number of parameters which serve to characterize the state of the active medium. These parameters are of familiar use in laser problems, and appear throughout this article. Section III starts by describing the statistical nature of the input incoherent radiation which is taken to be Gaussian. Since the statistics of the light are gradually modified by the nonlinear amplification process, we study the rate of change of fluctuations in intensity as a convenient measure of changes undergone by the initial distribution, and obtain theoretical expressions that are susceptible to experimental tests. In addition, the range of validity of Litvak's Gaussian statistics approximation is discussed with some detail.[9] Section IV begins with a numerical analysis of the equations applied to the case of fixed molecules (homogeneous broadening). The evolution of initially broadband Gaussian radiation toward quasimonochromatic oscillations and laserlike statistics is explored in several numerical examples. This section also includes a stability test of the monochromatic solution, and clearly establishes interesting connections of this study with that of Risken and Nummedal on self-pulsing in a ring laser configuration.[16]

In Sec. V, we consider the important case of broad-line oscillations in Doppler-broadened media. Spectral narrowing and rebroadening effects are discussed both analytically and with numerical examples. These examples show the distinct contribution of saturation, and pulsations in the population which give rise to mode-coupling phenomena (called Raman-type terms, in several articles[9,10,17]). If population pulsations are neglected, our expressions for the spectral narrowing-rebroadening rate reduce to forms previously obtained by Casperson and Yariv.[7] In general, however, mode-coupling effects can significantly alter the rebroadening process as well as the spectrum, and should not be ignored. The expressions should, then, be checked out with more detailed observations in nonlinear amplifiers. Numerical examples in Sec. V were compared with similar results obtained using Litvak's approach.[9] The differences we found, in conjunction with results of Sec. III C, indicate that—in laser amplifiers—the Gaussian approximation may be valid only for nonsaturated media. Finally, every numerical case of noise propagation is also compared with the propagation of a pulse having the same starting spectrum, but correlated phases ("coherent history," as opposed to "incoherent histories" where the phases are randomly selected.)

II. FIELD-MEDIUM COUPLED EQUATIONS

The effect of the electromagnetic field on the atoms of the active medium has been described elsewhere.[18] Briefly, the model for the active medium is taken to be a collection of two-level atoms in thermal motion, and coupled only through their dipole interaction with the overall field. The latter will be considered to be linearly polarized in the x direction and propagating along z,

$$\vec{E}(\vec{r}, t) = E(z, t)\hat{x}\,, \tag{2.1}$$

the field is then represented by a scalar $E(z, t)$. The frequency of the transition between levels a and b is designated by $\omega = (\omega_a - \omega_b) > 0$, and both levels are allowed to decay to lower states at rates indicated by $\gamma_a, \gamma_b \ll \omega$. Furthermore, it is assumed that the atoms are being steadily excited to a or b by some unspecified homogeneous pumping mechanism at rates

$$\lambda_\alpha = \Lambda_\alpha W(v), \quad \alpha = a \text{ or } b\,, \tag{2.2}$$

where Λ_α is the number of atoms of mass M excited to state α per unit volume and unit time, and $W(v)$ is the velocity distribution, e.g.,

$$W(v) = (\pi^{1/2}u)^{-1} \exp[-(v/u)^2], \quad u^2 = (2k_BT/M)\,. \tag{2.3}$$

The calculation scheme may be summarized as follows: The electric field $E(z, t)$ polarizes the atoms according to the laws of quantum mechanics, and the atomic dipole moments statistically add up to a macroscopic polarization $P(z, t)$, which enters as a source term into Maxwell's equations for the field.

All the macroscopic quantities we shall deal with, such as polarization $P(z, t, v)$ and popula-

tion-inversion density $D(z, t, v)$ for atoms of a given velocity v, can be expressed in terms of a population matrix $\underline{\rho}(z, t, v)$ for the two-level (a and b) system[15,18]:

$$P(z, t) = \int P(z, t, v)\, dv = \wp[\rho_{ab}(z, t, v) + \rho_{ba}(z, t, v)]\, dv, \quad (2.4)$$

$$D(z, t) = \int D(z, t, v)\, dv = \int [\rho_{aa}(z, t, v) - \rho_{bb}(z, t, v)]\, dv, \quad (2.5)$$

where $\wp$ (assumed real) is the matrix element of the atomic dipole operator between a and b.

The coupled equations of motion for $\underline{\rho}(z, t, v)$ and $E(z, t)$ have been discussed by a number of authors,[2,15,19] and for completeness are shown in Appendix A. These equations are reduced on the basis of a few, additional assumptions.

(i) Discussion will be limited to a "noise-amplifier configuration" with noise generated externally ($z < 0$). The noise that is generated internally in the amplifier (e.g., spontaneous emission) is often a weak source for many laboratory amplifiers,[7] as well as for interstellar masers,[9] and its inclusion will not appreciably alter the results. The light will be taken to be a unidirectional running wave of the form

$$E(z, t) = \tfrac{1}{2}[\mathcal{E}(z, t) e^{i(Kz - \omega t)} + \text{c.c.}], \quad (2.6)$$

where $K = \omega/c$. Note that a choice of a different frequency ν, instead of ω, in the phase factor of (2.6) would simply lead to a different phase for the complex amplitude $\mathcal{E}(z, t) = |\mathcal{E}(z, t)| e^{-i\phi(z,t)}$.

(ii) In order that the reflected wave may be neglected, we shall have to assume that the properties of the medium vary only slightly over a wavelength. In addition, it is assumed that the amplitude $|\mathcal{E}(z, t)|$, and phase $\phi(z, t)$, are slowly varying functions of t compared with $e^{i\omega t}$. Hence,

$$\frac{\partial |\mathcal{E}(z, t)|}{\partial z} \ll K |\mathcal{E}(z, t)|, \quad \frac{\partial |\mathcal{E}(z, t)|}{\partial t} \ll \omega |\mathcal{E}(z, t)|, \quad (2.7)$$

and similarly for $\phi(z, t)$. If higher harmonics are neglected, $\rho_{ab}(z, t, v)$ can be written in the same manner as the field; i.e.,

$$\rho_{ab}(z, t, v) = \tfrac{1}{2}[-i\rho(z, t, v)] e^{i(Kz - \omega t)}, \quad (2.8)$$

where the factor $(-i)$ has been included for convenience. Because of the refractive properties of the active medium, the slowly varying amplitude $[-i\rho(z, t, v)]$, in general consists of a part in phase with $\mathcal{E} = |\mathcal{E}| e^{-i\phi}$, and a part in quadrature.

(iii) Generation of rapid pulsations in $\rho_{aa}(z, t, v)$ and $\rho_{bb}(z, t, v)$ will be neglected by making a rotating wave approximation. Then, $\rho_{aa}(z, t, v)$, $\rho_{bb}(z, t, v)$ as well as $\rho(z, t, v)$, are slowly varying and satisfy relations of the type (2.7).

A. Field-medium equations: Time domain

With considerations (i)–(iii) taken into account, the coupled equations of Appendix A adopt the following form in terms of the slowly varying quantities (∂_t, ∂_z indicate partial derivatives):

$$(\partial_t + c\partial_z)\mathcal{E}(z, t) = -\tfrac{1}{2} c\kappa \mathcal{E}(z, t) + \frac{1}{2} \frac{\omega \wp}{\epsilon_0} \int \rho(z, t, v)\, dv, \quad (2.9)$$

$$(\partial_t + v\partial_z)\rho_{aa}(z, t, v) = \lambda_a - \gamma_a \rho_{aa} - \tfrac{1}{4}(\wp/\hbar)[\mathcal{E}^* \rho + \mathcal{E} \rho^*], \quad (2.10)$$

$$(\partial_t + v\partial_z)\rho_{bb}(z, t, v) = \lambda_b - \gamma_b \rho_{bb} + \tfrac{1}{4}(\wp/\hbar)[\mathcal{E}^* \rho + \mathcal{E} \rho^*], \quad (2.11)$$

$$(\partial_t + v\partial_z)\rho(z, t, v) = -\gamma_{ab} \rho - iKv\rho + (\wp/\hbar)\mathcal{E}[\rho_{aa} - \rho_{bb}]. \quad (2.12)$$

The second term in the "substantial" derivative $(\partial_t + v\partial_z)$ is responsible for the Doppler-shift term $-iKv\rho$. Now, we are in a position to neglect $v\partial_z$, because for thermal velocities, $v \ll c$, and $v\partial_z \approx (v/c)\partial_t \ll \partial_t$.[20]

Given initial conditions $\rho(z, 0, v)$, $\rho_{\alpha\alpha}(z, 0, v)$ for the medium, and the boundary condition $\mathcal{E}(0, t)$ for the field, Eqs. (2.9)–(2.12) in principle determine $\mathcal{E}(z, t)$ for any z, t. Since $\mathcal{E}(z, t)$, $\rho(z, t, v)$, and $\rho_{\alpha\alpha}(z, t, v)$ do not change much in a time $1/\omega$, the equations may be used in a wide range of physical situations: from long signals, with duration $\Delta t \gg \gamma_\alpha^{-1} \gg \omega^{-1}$, to ultrashort ones, $\gamma_\alpha^{-1} \gg \Delta t \gg \omega^{-1}$. The spectral widths ($\Delta\nu \sim \Delta t^{-1}$) vary accordingly from $\Delta\nu \ll \gamma_\alpha \ll \omega$, to $\gamma_\alpha \ll \Delta\nu \ll \omega$.

The radiation hitting the entry plane at $z = 0$, e.g., white noise or blackbody radiation, might be regarded as a sequence of distrubances occurring at random, and produced by a great many independent sources.[21] Therefore, the light field is not characterized by a given function $\mathcal{E}(z, t)$; but rather by a stochastic variable; i.e., $\mathcal{E}(z, t)$ is a member of a statistical ensemble and corresponds to a possible realization of the field. Equations (2.9)–(2.12) which are particularly useful for describing pulse-propagation phenomena, have been also used in the time-domain analysis of noise amplification in a nonlinear medium.[13,22] In this case, noise at $z = 0$ is considered as a very long input "pulse" $\mathcal{E}(0, t)$, whose value at discrete t points are selected within some prescribed probability distribution. The calculations are, then, of the form of an extended pulse-propagation calculation. Power

spectra is finally obtained by Fourier analysis of correlation functions $\langle \mathcal{E}(z, t)\mathcal{E}^*(z, t+\tau)\rangle$. In practice, only a small, temporal sample of the output can be generated.

B. Field-medium equations: Frequency domain

Since our primary concern is the spectrum of the amplified radiation, it is preferable to work from the onset in the frequency domain. The representation of noise disturbances by means of Fourier series goes back many years: Lord Rayleigh suggested it for white-light representation, Einstein and von Laue have discussed the normal distribution of the random spectral amplitudes in Fourier series representing blackbody radiation.[21] Similarly, we assume here that the field (2.6) is periodic with some arbitrary period T and write

$$\mathcal{E}(z, t)e^{i(Kz-\omega t)} = \sum_{n=-\infty}^{+\infty} [\mathcal{E}_n(z)e^{i\nu_n z/c}]e^{-i\nu_n t},$$
$$= e^{i(Kz-\omega t)} \sum_{n=-\infty}^{+\infty} [\mathcal{E}_n e^{i(\nu_n-\omega)z/c}] \times e^{-i(\nu_n-\omega)t}, \quad (2.13)$$

where the inverse Fourier amplitudes are given by

$$\mathcal{E}_n(z)e^{i\nu_n z/c} = (1/T)\int_{-T/2}^{+T/2} [\mathcal{E}(z, t)e^{i(Kz-\omega t)}]e^{i\nu_n t}\, dt, \quad (2.14)$$

and where

$$K = \omega/c, \quad \nu_n = nf, \quad f = 2\pi/T. \quad (2.15)$$

For convenience, the amplitudes are shown with factors $\exp(i\nu_n z/c)$, and ω is assumed to be one of the ν_n's. In principle, if not in practice, the period T may be allowed to become arbitrarily large.[23]

Dealing with noise, the customary way of looking at representation (2.13) is as follows. Suppose, for example at $z=0$, we have an oscillogram of $E(0, t)$ extending from $t=0$ to $t=\infty$. The oscillogram may be cut up into strips of length T. A Fourier analysis of each strip provides a set of amplitudes $\mathcal{E}_n(0) = |\mathcal{E}_n(0)|e^{i\phi_n(0)}$ with uncorrelated phases; these amplitudes will vary randomly from strip to strip. The representation (2.13) assumes that this variation is governed by a distribution appropriate to the statistical properties of the radiation, e.g., at $z=0$, uniformly distributed random phases and a normal distribution of amplitudes with a standard deviation determined by the power spectrum. In other words, the statistical ensemble may be regarded as consisting of the strip collection; and if $\langle\ \rangle$ denotes ensemble average, $I_n(0) = |\mathcal{E}_n(0)|^2$ will usually fluctuate around the average value $\langle I_n(0)\rangle$, which itself may vary with n, while $\phi_n(0)$ will also undergo fluctuations between $(0, 2\pi)$.

The atomic medium response to the presence of the chaotic field may also be represented by Fourier series,

$$\rho(z, t, v)e^{i(Kz-\omega t)} = \sum_{n=-\infty}^{+\infty} [\rho_n(z, v)e^{i\nu_n z/c}]e^{-i\nu_n t}, \quad (2.16)$$

$$D(z, t, v) = \rho_{aa} - \rho_{bb} = \sum_{m=-\infty}^{+\infty} [D_m(z, v)e^{i\nu_m z/c}]e^{-i\nu_m t}, \quad (2.17)$$

$$D_{-m} = D_m^* \quad (2.18)$$

since $D(z, t, v)$ is real.

Similarly, we will have use for the Fourier series representation of the power per unit volume,[20] delivered to the field by atoms of velocity v,

$$(\tfrac{1}{4}\omega\wp)[\mathcal{E}^*(z, t)\rho(z, t, v) + \text{c.c.}]$$
$$= (\tfrac{1}{4}\omega\wp)\sum_{m=-\infty}^{+\infty}\Big[\sum_q \Big(\mathcal{E}_q^*(z)\rho_{q+m}(z, v) + \mathcal{E}_q(z)\rho_{q-m}^*(z, v)\Big) \times e^{i\nu_m z/c}\Big]e^{-i\nu_m t}. \quad (2.19)$$

The dc pumping terms (2.2) are also given the form

$$\lambda_\alpha = \Lambda_\alpha W(v)\sum_m (\delta_{m,0}e^{i\nu_m z/c})e^{-i\nu_m t}. \quad (2.20)$$

The series (2.13) and (2.16)–(2.20), are inserted into Eqs. (2.9)–(2.12), and one obtains a set of coupled equations for the Fourier amplitudes that couple $\mathcal{E}_n(z)$ with $\rho_n(z, v)$ and $D_m(z, v)$ (see Appendix B). Next, these equations will be given a more convenient form.

For numerical analysis purposes, we will consider a model with discrete atomic velocities

$$Kv_j = jf, \quad (2.21)$$

where j is an integer, and f is the frequency interval defined by (2.15). It could be a different one $f_v \neq f$, but the essential physical features are still present and computer evaluations of (B1)–(B3) are simplified. Note that the Doppler-shift Kv_j frequencies are congruent with the discrete frequencies of the spectrum. A convenient velocity distribution is

$$\mathcal{W}(j) = (N_W)^{-1}\exp[-(jf/Ku)^2](f/Ku),$$
$$N_W = \sum_j \exp[-(jf/Ku)^2](f/Ku). \quad (2.22)$$

The distribution (2.22) is already normalized, $\sum\mathcal{W}(j) = 1$, and takes the appropriate limiting forms in the case of homogeneous broadening ($u \to 0$), where $\lim\mathcal{W}(j) = \delta_{j,0}$, and in the continuous spec-

trum case ($f = K\Delta v \to 0$), where

$$\lim N_W = \int_{-\infty}^{+\infty} \exp[-(v/u)^2]\, d(v/u) = \pi^{1/2}$$

and

$$\lim \mathcal{W}(j) = (\pi^{1/2}u)^{-1} \exp[-(v/u)^2]\, dv = W(v)\, dv\,.$$

Concurrently with (2.21) and (2.22), the velocity-dependent amplitudes are changed to

$$\rho_n(z,j) = \rho_n(z, v_j)\Delta v, \quad D_m(z,j) = D_m(z, v_j)\Delta v\,,$$

with $\Delta v = f/K$. Equations (B1) – (B3) are given a more compact form by defining a few constants of familiar use in laser theory.[15] These are

$$N_0 = (\Lambda_a/\gamma_a) - (\Lambda_b/\gamma_b)\,, \tag{2.23}$$

which is the steady-state inverted population density established by the pumping in the absence of the radiation field,

$$\gamma = [\tfrac{1}{2}(1/\gamma_a + 1/\gamma_b)]^{-1} \tag{2.24}$$

with dimensions of a rate,

$$\beta = \sum_j \mathcal{W}(j)\, \frac{(\gamma_{ab}/f)^2}{(\gamma_{ab}/f)^2 + j^2} = \sum_j \mathcal{W}(j)\mathfrak{L}(j)\,, \tag{2.25a}$$

which is a dimensionless average of the Doppler-shifted Lorentzian atomic response (at $\nu_n = \omega$), over the velocity distribution. For $\Delta v = f/Ku \to 0$,

$$\beta = (\gamma_{ab}/Ku) Z_i(0, \gamma_{ab}/Ku)\,, \tag{2.25b}$$

where Z_i is the imaginary part of the plasma dispersion function.[19, 24] In the absence of atomic motion [$\mathcal{W}(j) = \delta_{j,0}$] $\beta = 1$, otherwise $\beta < 1$.[25] Another constant of familiar use in laser theory is

$$G = (\omega \wp^2 N_0/c\epsilon_0 \hbar \gamma_{ab})\beta = G_0\beta\,, \tag{2.26}$$

which has dimensions of a reciprocal length and represents the linear gain of a weak monochromatic signal at resonance with the atomic transition $\nu_n = \omega$. G_0 is the linear gain when there is no atomic motion ($u = 0$). In addition, a further simplification is achieved by working with quantities which are proportional to $\mathcal{E}_n$, ρ_n, and D_m. This is accomplished by the assignments

$$\left(\frac{\wp\, \mathcal{E}_n(z)}{\hbar(\gamma\gamma_{ab})^{1/2}}\right) \to \mathcal{E}_n, \quad \left(\frac{\rho_n(z,j)\gamma_{ab}}{N_0(\gamma\gamma_{ab})^{1/2}}\right)\beta^{-1} \to \rho_n\,,$$

$$\left(\frac{D_m(z,j)}{N_0}\right) \to D_m\,. \tag{2.27}$$

Note that the new $\mathcal{E}_n(z)$, $\rho_n(z,j)$, and $D_n(z,j)$ are all dimensionless.[26]

The field-medium equations in the frequency domain are finally given the form

$$\partial_z \mathcal{E}_n(z) = -\tfrac{1}{2}\kappa\, \mathcal{E}_n(z) + \tfrac{1}{2} G \sum_j \rho_n(z,j)\,, \tag{2.28}$$

$$\rho_n(z,j) = \beta^{-1}\mathfrak{D}(n-j) \sum_l \mathcal{E}_l(z) D_{n-l}(z,j)\,, \tag{2.29}$$

$$D_m(z,j) = \mathcal{W}(j)\delta_{m,0} - \tfrac{1}{2}\beta\, \mathfrak{F}(m) \sum_q [\mathcal{E}_q^* \rho_{q+m} + \mathcal{E}_q \rho_{q-m}^*]\,, \tag{2.30}$$

where

$$\mathfrak{D}(n-j) = \frac{\gamma_{ab}/f}{(\gamma_{ab}/f) - i(n-j)}, \tag{2.31}$$

$$\mathfrak{F}(m) = \tfrac{1}{2}\left(\frac{\gamma/f}{(\gamma_a/f) - im} + \frac{\gamma/f}{(\gamma_b/f) - im}\right), \quad \mathfrak{F}(0) = 1\,, \tag{2.32}$$

and where the origin for the frequencies has been shifted to ω by taking $(\nu_n - \omega) = nf$ [see (2.13)]. In Appendix C, we outline one of several methods that can be used for numerical analysis of (2.28)–(2.30), see Eqs. C9–C12.

The above coupled equations govern the behavior of any member of the ensemble (i.e., a generic T strip). The picture of an ensemble consisting of many observation periods of length T can be imitated by repeated numerical solutions of (2.28)–(2.30), each time with a different set of starting conditions. Typically, the individual calculations are extremely lengthy, and in actual computer work one deals with a restricted number of histories. In some cases, the results are obvious on inspection, even for a small sample. In some other cases, the results obtained from small samples are overwhelmed by fluctuations. For this reason, a theory dealing with the propagation of the power spectrum, $\langle I_n(z)\rangle = \langle \mathcal{E}_n^*(z)\mathcal{E}_n(z)\rangle$, inside the noise amplifier would be very useful, and it has been sought by several authors.[9, 10, 27] Obviously, an adequate approach along this idea should start from the basic set (2.28)–(2.30); for example, the transport equation for the power spectrum can be obtained from (2.28) and its c.c. After ensemble average we get

$$\frac{d}{dz}\langle I_n(z)\rangle = -\kappa\langle I_n(z)\rangle + \tfrac{1}{2} G \sum_j [\langle \mathcal{E}_n^*(z)\rho_n(z,j)\rangle + \text{c.c.}]\,. \tag{2.33}$$

From Eq. (2.19) we know that the second term on the right-hand side of (2.33) represents the average power delivered to the field at frequency $\nu_n = nf$, by atoms of different velocities $v_j = (jf/Ku)$. The quantity, $\langle \mathcal{E}_n^*(z)\rho_n(z,j)\rangle$ needs evaluation at every step z into the medium; however, in the next section we show that this is not generally possible, because the nonlinear medium changes the statistics of the input incoherent radiation.

III. STATISTICS OF THE RADIATION FIELD: PROPAGATION OF THE POWER SPECTRUM

A. Nature of the input incoherent radiation

We begin by specifying the statistical nature of the incoherent radiation hitting the entry plane ($z=0$). The radiation field generated by a thermal source is a well-known example of noise, in which the ensemble distribution of each amplitude is Gaussian. Let $d^2\mathcal{E}_k$ be the area element in the complex $\mathcal{E}_k$ plane; i.e., $d^2\mathcal{E}_k = d(\mathrm{Re}\,\mathcal{E}_k)\, d(\mathrm{Im}\,\mathcal{E}_k) = \frac{1}{2} d\,|\mathcal{E}_k|^2 d\phi_k$. Then, the probability distribution for the set $\{\mathcal{E}_k\}$ of random, independent amplitudes, is given by an expression of the type[28,29]

$$P(\{\mathcal{E}_k\}) = \prod_k \Phi(\mathcal{E}_k) d\,|\mathcal{E}_k|^2 d\phi_k\,, \tag{3.1a}$$

where

$$\Phi(\mathcal{E}_k) = (2\pi\langle\,|\mathcal{E}_k|^2\rangle)^{-1} \times \exp\left[\frac{-|\mathcal{E}_k|^2}{\langle|\mathcal{E}_k|^2\rangle}\right] d\,|\mathcal{E}_k|^2 d\phi_k \tag{3.1b}$$

are normalized by

$$\int_0^{2\pi} d\phi_k \int_0^{\infty} \Phi(\mathcal{E}_k) d\,|\mathcal{E}_k|^2 = 1\,. \tag{3.1c}$$

Note that $(\frac{1}{2}\pi)$ is the uniform probability distribution for ϕ_k, whereas $(\langle I_k\rangle)^{-1}\exp[-I_k/\langle I_k\rangle]$ is the distribution for I_k.[30] As suggested by Glauber,[29] the Gaussian distribution should describe not only thermal light, but is presumably characteristic of many noncoherent macroscopic light sources not necessarily in thermal equilibrium (e.g., gas discharge tubes).

An exclusive feature of Gaussian processes is that they are completely determined by their first and second moments; for example, using (3.1) one can see that

$$\langle \mathcal{E}_k^* \mathcal{E}_k \mathcal{E}_n^* \mathcal{E}_n\rangle = \langle\, \mathcal{E}_k^* \mathcal{E}_k\rangle\langle \mathcal{E}_n^* \mathcal{E}_n\rangle, \quad k \neq n\,, \tag{3.2}$$

$$\langle \mathcal{E}_n^* \mathcal{E}_n \cdots (p \text{ times}) \cdots \mathcal{E}_n^* \mathcal{E}_n\rangle = p!\,[\langle I_n\rangle]^p\,. \tag{3.3}$$

In general, if F is an arbitrary function of the set $\{\mathcal{E}_k$'s$\}$,

$$\langle \mathcal{E}_n^* \mathcal{E}_n F(\{\mathcal{E}_k\text{'s}\})\rangle = \langle I_n\rangle\langle F\rangle + [\langle I_n\rangle]^2 \frac{\partial\langle F\rangle}{\partial\langle I_n\rangle}\,, \tag{3.4}$$

which is obtained by simple derivation of

$$\langle F\rangle = \int \cdots \int F \prod_j \Phi(I_j) dI_j d\phi_j$$

in conjunction with (3.1). In actual computer work, a set of random numbers obeying a probability distribution such as (3.1) can be obtained from the random number generator which provides a sequence of uniformly distributed random real numbers, x, between 0 and 1. For example, if $\mathfrak{U}(x) = 1$, $0 \leq x \leq 1$, denote the uniform probability distribution for x; and

$$\mathcal{P}(I_k) = \langle I_k\rangle^{-1} \exp[-I_k/\langle I_k\rangle]$$

the distribution for I_k. Then, by equating the probabilities

$$\int_0^{I_k} \mathcal{P}(I_k)\, dI_k = \int_0^x \mathfrak{U}(x)\, dx = x\,,$$

we readily obtain that the numbers determined by

$$I_k(x) = -\langle I_k\rangle \ln(1-x) \tag{3.5}$$

will be distributed according to $\mathcal{P}(I_k)$. Similarly, $\phi(x) = [2\pi x - \pi]$, will be uniformly distributed between $(-\pi, \pi)$.

From (3.1), one can readily see that

$$\langle \mathcal{E}_k^*(0)\, \mathcal{E}_n(0)\rangle = \langle I_n(0)\rangle \delta_{n,k}\,. \tag{3.6}$$

The above relation indicates that within the ensemble, the phases of any two different spectral components are uncorrelated.[31] If at the input ($z=-0$), the incoherent radiation satisfies (3.6), it is to be expected that similar relations will hold at $z \geq +0$, i.e.,

$$\langle \mathcal{E}_n^*(z)\, \mathcal{E}_k(z)\rangle = \langle I_n(z)\rangle \delta_{n,k}\,, \tag{3.7}$$

$$\langle \mathcal{E}_n^*(z) \rho_k(z)\rangle = \langle \mathcal{E}_n^*(z) \rho_n(z)\rangle \delta_{n,k}\,, \tag{3.8}$$

this is shown—for small signals—in Appendix D. In other words, the relations (3.7), (3.8) in conjunction with the Fourier-series representation (2.13)–(2.19), imply that the statistics will preserve its "stationary" character during propagation.[31,32] On the other hand, we will show that the Gaussian features of the starting distribution will not remain unchanged at $z > 0$, especially when intensities are large and nonlinearities become important.[33]

B. Propagation of the power spectrum: Litvak's equations

Let us return to Eq. (2.33) for the propagation of the power spectrum; i.e.,

$$\frac{d}{dz}\langle I_n(z)\rangle = -\kappa\langle I_n(z)\rangle + \tfrac{1}{2} G \sum_j [\langle \mathcal{E}_n^*(z)\, \rho_n(z,j)\rangle + \text{c.c.}]\,.$$

We shall now see that the above equation has a limited utility in noise amplifier problems, because an adequate computation of $\langle \mathcal{E}_n^*(z)\, \rho_n(z,j)\rangle$ requires a complete knowledge of the statistics at every place z into the atomic medium. Therefore, at least in principle, there are disadvantages in dealing with (2.33), as opposed to repeated numerical solutions of the basic set of Eqs. (2.28)–(2.30), for an ensemble of different starting histories.

To evaluate $\langle \mathcal{E}_n^* \rho_n \rangle$ we start from Eq. (2.29) for $\rho_n(z,j)$; multiplying by $\mathcal{E}_n^*(z)$ and averaging over the ensemble we get

$$\langle \mathcal{E}_n^*(z)\rho_n(z,j)\rangle = \beta^{-1}\mathfrak{D}(n-j)\left(\langle \mathcal{E}_n^*\mathcal{E}_n D_o\rangle + \sum_{l(\neq n)}\langle \mathcal{E}_n^*\mathcal{E}_l D_{n-l}\rangle\right), \quad (3.9)$$

where for convenience we separate the saturation term from the mode-coupling terms. The D_m's given by Eq. (2.30) are now substituted into (3.9). Since the phases of two distinct Fourier components are uncorrelated at any depth z [Eqs. (3.7) and (3.8)], we see that there is only one term in $D_{n-l}(l\neq n)$ giving a nonzero contribution at the right-hand side of (3.9). This term is

$$-\tfrac{1}{2}\beta\mathfrak{F}(n-l)[\mathcal{E}_l^*\rho_n + \mathcal{E}_n\rho_l^*],$$

and (3.9) will, then, adopt the form

$$\langle \mathcal{E}_n^*(z)\rho_n(z,j)\rangle = \beta^{-1}\mathfrak{D}(n-j)\Big(\mathfrak{W}(j)\langle \mathcal{E}_n^*\mathcal{E}_n\rangle - \tfrac{1}{2}\beta\sum_q[\langle \mathcal{E}_n^*\mathcal{E}_n\mathcal{E}_q^*\rho_q\rangle + \langle \mathcal{E}_n^*\mathcal{E}_n\mathcal{E}_q\rho_q^*\rangle]$$
$$-\tfrac{1}{2}\beta\sum_{l(\neq n)}\mathfrak{F}(n-l)[\langle \mathcal{E}_n^*\mathcal{E}_l\mathcal{E}_l^*\rho_n\rangle + \langle \mathcal{E}_n^*\mathcal{E}_l\mathcal{E}_n\rho_l^*\rangle]\Big). \quad (3.10)$$

The expression (3.10) shows that $\langle \mathcal{E}_n^*(z)\rho_n(z,j)\rangle$ depends on a hierarchy of higher-order correlations such as $\langle \mathcal{E}_n^*\mathcal{E}_n\mathcal{E}_q^*\rho_q\rangle$, and so on. This means that a computation of $\langle \mathcal{E}_n^*(z)\rho_n(z,j)\rangle$ requires a full knowledge of the statistics at the place z.

In an effort to overcome the above difficulty, several authors,[9,10,12,27] assume that the Gaussian features of the input distribution remain nearly unchanged during propagation. The statistics are then determined by the first and second moments, and (3.10) has been given the form

$$\langle \mathcal{E}_n^*(z)\rho_n(z,j)\rangle \approx \beta^{-1}\mathfrak{D}(n-j)\Big(\mathfrak{W}(j)\langle I_n\rangle - \tfrac{1}{2}\beta\langle I_n\rangle\sum_q[\langle \mathcal{E}_q^*\rho_q\rangle + \langle \mathcal{E}_q\rho_q^*\rangle]$$
$$-\tfrac{1}{2}\beta\sum_l\mathfrak{F}(n-l)[\langle I_l\rangle\langle \mathcal{E}_n^*\rho_n\rangle + \langle I_n\rangle\langle \mathcal{E}_l\rho_l^*\rangle]\Big), \quad (3.11)$$

by factoring out high-order correlations in pairwise second-order correlations. For example, the second line in (3.11) is simply $\langle \mathcal{E}_n^*\mathcal{E}_n\rangle\langle D_o\rangle$, as opposed to $\langle \mathcal{E}_n^*\mathcal{E}_n D_o\rangle$ appearing in (3.10). Equation (3.11) with $f\to d\nu$ and $nf\to\nu$, may be readily recognized as equivalent to Eq. (8) of Litvak's article.[9]

Dealing with noise amplifiers, there are two reasons which indicate that the validity of Eq. (3.11) is questionable beyond the small signal regime. First, even if the statistics are Gaussian, the factorization used in the transition from (3.10) to (3.11), e.g.,

$$\langle \mathcal{E}_n^*\mathcal{E}_n\mathcal{E}_q^*\rho_q\rangle \to \langle I_n\rangle\langle \mathcal{E}_q^*\rho_q\rangle, \quad q\neq n$$
$$= 2\langle I_n\rangle\langle \mathcal{E}_n^*\rho_n\rangle, \quad q=n$$
$$\langle \mathcal{E}_n^*\mathcal{E}_n D_o\rangle \to \langle I_n\rangle\langle D_o\rangle,$$

is not strictly valid because ρ_q (or D_o) is a nonlinear function of the field amplitudes: $\rho_q \approx \rho_q^{(1)} + \rho_q^{(3)} + \rho_q^{(5)} + \cdots$. The above factorization procedure, implicitly assumes that $\langle \mathcal{E}_q^*\rho_q\rangle$ (or $\langle D_o\rangle$) does not depend on $\langle I_n\rangle$; however, this is true only in the first approximation $\rho_q \approx \rho_q^{(1)} \propto \mathcal{E}_q$. In other words, if one assumes Gaussian statistics, and applies the correct factorization procedure (3.4) to Eq. (3.10), it is not difficult to show that Litvak's equation (3.11) only holds up to the fourth order in the field amplitudes. In practice, the factorization used in Litvak's equations may still be a good approximation at large signals since it provides the leading terms. However, the validity of (3.11) is still questionable because of a second, more important reason: after the initial stages of noise amplification, nonlinear effects such as saturation and mode-coupling phenomena gradually change the statistical nature of the input distribution, and the Gaussian assumption is simply not true beyond the small signal regime. This is shown next.

C. Rate of change of fluctuations in intensity

A *convenient* measure of the change in statistics can be obtained by studying the rate of change of fluctuations in intensity,

$$\mathcal{Q}_n(z) = \frac{\langle [I_n(z)]^2\rangle - [\langle I_n(z)\rangle]^2}{[\langle I_n(z)\rangle]^2}. \quad (3.12)$$

At $z=0$, where the statistics are Gaussian, Eq. (3.3) shows that $\mathcal{Q}_n(0)=1$. By taking the derivative of (3.12), we can write the fluctuations rate of change as

$$\frac{d\mathcal{Q}_n(z)}{dz} = \frac{1}{\langle I_n\rangle^2}\left(\frac{d}{dz}\langle I_n^2\rangle - 2\frac{\langle I_n^2\rangle}{\langle I_n\rangle}\frac{d}{dz}\langle I_n\rangle\right); \quad (3.13)$$

and we are in a position to explicitly evaluate $[d\mathcal{Q}_n(z)/dz]_{z=0}$, because, there, the statistical distribution is well defined.

The two terms of (3.13) are obtained in the same way as Eq. (2.33), i.e.,

$$\frac{d}{dz}\langle I_n^2\rangle = -2\kappa\langle I_n^2\rangle + G\sum_j [\langle I_n \mathcal{E}_n^* \rho_n\rangle + \text{c.c.}], \tag{3.14}$$

$$2\frac{\langle I_n^2\rangle}{\langle I_n\rangle}\frac{d}{dz}\langle I_n\rangle = -2\kappa\langle I_n^2\rangle + \frac{\langle I_n^2\rangle}{\langle I_n\rangle} G\sum_j [\langle \mathcal{E}_n^* \rho_n\rangle + \text{c.c.}], \tag{3.15}$$

More explicit expressions for the right-hand side of both (3.14) and (3.15) are obtained by the same procedure that lead to (3.9)–(3.10). We write the final result for (3.13) as

$$\begin{aligned}\frac{d\mathcal{Q}_n(z)}{dz} = \frac{G}{\langle I_n\rangle^2}\Big[&-\sum_j \mathfrak{L}(n-j)\sum_q [\langle I_n^2 \mathcal{E}_q^* \rho_q\rangle + \langle I_n^2 \mathcal{E}_q \rho_q^*\rangle] + \sum_j \mathfrak{L}(n-j)\sum_q \frac{\langle I_n^2\rangle}{\langle I_n\rangle}[\langle I_n \mathcal{E}_q^* \rho_q\rangle + \langle I_n \mathcal{E}_q \rho_q^*\rangle] \\ &- \sum_j \Big(\mathfrak{D}(n-j)\sum_{l\neq n} \tfrac{1}{2}\mathfrak{F}(n-l)[\langle I_n \mathcal{E}_n^* \rho_n I_l\rangle + \langle I_n^2 \mathcal{E}_l \rho_l^*\rangle] + \text{c.c.}\Big) \\ &+ \sum_j \Big(\mathfrak{D}(n-j)\sum_{l\neq n} \tfrac{1}{2}\mathfrak{F}(n-l)\frac{\langle I_n^2\rangle}{\langle I_n\rangle}[\langle \mathcal{E}_n^* \rho_n I_l\rangle + \langle I_n \mathcal{E}_l \rho_l^*\rangle] + \text{c.c.}\Big)\Big],\end{aligned} \tag{3.16}$$

where

$$\mathfrak{L}(n-j) = \tfrac{1}{2}[\mathfrak{D}(n-j) + \mathfrak{D}^*(n-j)] = \frac{(\gamma_{ab}/f)^2}{(\gamma_{ab}/f)^2 + (n-j)^2}. \tag{3.17}$$

As expected, the terms due to linear gain and losses in (3.14) and (3.15), do not appear in (3.16) since only nonlinear effects can change the statistics. The first two terms at the right-hand side account for saturation effects, while the last two are contributions due to mode coupling.

Note that the terms within the square brackets at the right-hand side of (3.16), are at least of sixth order in the field amplitudes. During the initial stages of noise amplification, a good approximation can be obtained by neglecting population pulsations, $|D_m| \ll D_o$. That is, substituting ρ_q by

$$\rho_q(z,j) \approx \beta^{-1}\mathfrak{D}(q-j)\,\mathcal{E}_q D_o(z,j),$$

with

$$D_o(z,j) \approx \mathfrak{W}(j)\Big(1 + \sum_k I_k \mathfrak{L}(k-j)\Big)^{-1}.$$

Furthermore, since the starting ensemble is assumed to be Gaussian, one can use the factorization rules (3.2)–(3.4) to compute ensemble averages. If only the leading terms are kept, the main contribution to (3.16) comes from saturation terms $(q=n)$,

$$\begin{aligned}\frac{d\mathcal{Q}_n(z)}{dz}\Big|_{z\approx 0} &\approx -\frac{2G\beta^{-1}}{\langle I_n\rangle^2}\sum_j \Big(\langle I_n^3 D_o\rangle - \frac{\langle I_n^2\rangle}{\langle I_n\rangle}\langle I_n^2 D_o\rangle\Big)[\mathfrak{L}(n-j)]^2 \\ &\approx -4G\beta^{-1}\langle I_n\rangle\sum_j \langle D_o(j)\rangle[\mathfrak{L}(n-j)]^2;\end{aligned} \tag{3.18}$$

Eq. (3.18) indicates that fluctuations in intensity diminish with distance. The rate is more pronounced at the line center, and also for the homogeneous broadening case, $\mathfrak{W}(j) = \delta_{j,o}$,

$$\frac{d\mathcal{Q}_n}{dz}\Big|_{z\approx 0} \approx -4G_o\langle I_n\rangle\Big\langle\frac{1}{1+\sum_k I_k \mathfrak{L}(k)}\Big\rangle[\mathfrak{L}(n)]^2. \tag{3.19}$$

For moving atoms, Eq. (3.18) can be given a simple form in the Doppler-limit case $(Ku \gg \gamma_{ab})$, and provided that the spectrum remains broad compared with γ_{ab}. First, we write (3.18) more explicitly as

$$\begin{aligned}\frac{d\mathcal{Q}_n}{dz}\Big|_{z\approx 0} \approx &-4G\beta\langle I_n\rangle \\ &\times\sum_j \Big\langle\frac{\mathfrak{W}(j)}{1+\sum_k I_k \mathfrak{L}(k-j)}\Big\rangle \\ &\times\Big(1 - \tfrac{1}{2}\gamma_{ab}\frac{d}{d\gamma_{ab}}\Big)\mathfrak{L}(n-j),\end{aligned} \tag{3.20}$$

where the second term is a simple derivative of the first one. The Doppler limit can, now, be easily applied, and a similar calculation is described with some detail in Sec. V, Eq. (5.16). Here we only quote the final result,[25]

$$\frac{d\mathcal{Q}_n}{dz} \approx -2G\langle I_n\rangle\Big\langle\frac{1}{1+[\beta/\mathfrak{W}(0)]I_n}\Big\rangle\exp[-(\nu_n/Ku)^2], \tag{3.21}$$

where $\mathfrak{W}(0) \approx \pi^{-1/2}(f/Ku)$, and in the Doppler limit $\beta \approx \pi^{1/2}(\gamma_{ab}/Ku)$. If the Doppler limit does not apply, Eq. (3.20) can still be written in terms of the plasma dispersion function, and its derivative with respect to γ_{ab}/Ku.[19,24,34]

There are laboratory measurements dealing with statistical changes on amplified spontaneous emission (ASE),[35,36] and there seems to be qualitative

agreement between the present theory and these experiments; but more detailed measurements appear to be necessary for a strict comparison. On the other hand, some observations on the statistical properties of radiation from saturated OH astronomical masers, fail to indicate significant departures from Gaussian statistics. The authors, however, list several effects which may prevent the observation of such deviations.[11]

IV. EVOLUTION TOWARD QUASIMONOCHROMATIC OSCILLATIONS WITH LASERLIKE STATISTICS

A. Numerical analysis

This section begins with a computer integration of Eqs. (2.28)–(2.30) for a homogeneously broadened medium, $\mathcal{W}(j)=\delta_{j,o}$, with not too small values for the loss-gain ratio:

$$\mathcal{R}=\kappa/G_o\,,\quad 0<\mathcal{R}<1\ \text{(above threshold)}\,. \tag{4.1}$$

The conclusions are obtained from an ensemble consisting of a few different histories to which we applied the numerical method outlined in Appendix C. For every member of the ensemble, the boundary condition at $z=0$ is a low intensity, white spectrum, and starting every time with a different choice of initial random phases. The result was invariably a disappearance of the sidebands, and a building up of the central frequency toward a final, constant value predicted by coherent amplifier theory.[2,3,16] That is, the radiation undergoes spectral narrowing, and does tend towards a quasimonochromatic, steady-state output, with vanishing intensity fluctuations, as in a single mode laser: $\delta(I-\langle I\rangle)\,dI$. The steady-state values are easily obtained from Eqs. (2.28)–(2.30) for the homogeneous broadening case, if one applies the conditions for constant amplitude ($d/dz\equiv 0$) and single mode oscillations at the resonance frequency ($\mathcal{E}_n=\mathcal{E}_0\delta_{n,o}$, $\rho_n=\rho_o\,\delta_{n,o}$, $D_m=D_o\,\delta_{m,o}$),

$$0=-\mathcal{R}\mathcal{E}_o+\rho_o\,,$$

$$\rho_o=\mathcal{E}_o D_o\,,$$

$$D_o=1-\tfrac{1}{2}[\mathcal{E}_o^*\rho_o+\mathcal{E}_o\rho_o^*]\,,$$

which give

$$I_o=|\mathcal{E}_o|^2=(1-\mathcal{R})/\mathcal{R}\,,\quad D_o=1/(1+I_o)=\mathcal{R},$$
$$\rho_o=\mathcal{R}\mathcal{E}_o\,. \tag{4.2}$$

Figures 1(a) and 1(b) show the spectral evolution of one of the typical incoherent histories, for different depths into the medium. Depths are measured in dimensionless units of $G_0 z$. At $z=0$, the spectrum is taken to be "flat": $I_n(z=0)=2.5\times10^{-3}$ for $|n|\leq 10$, and $I_n(0)=2.5\times10^{-5}$ for $|n|>10$; while the phases $\phi_n(0)$'s are a random set with values

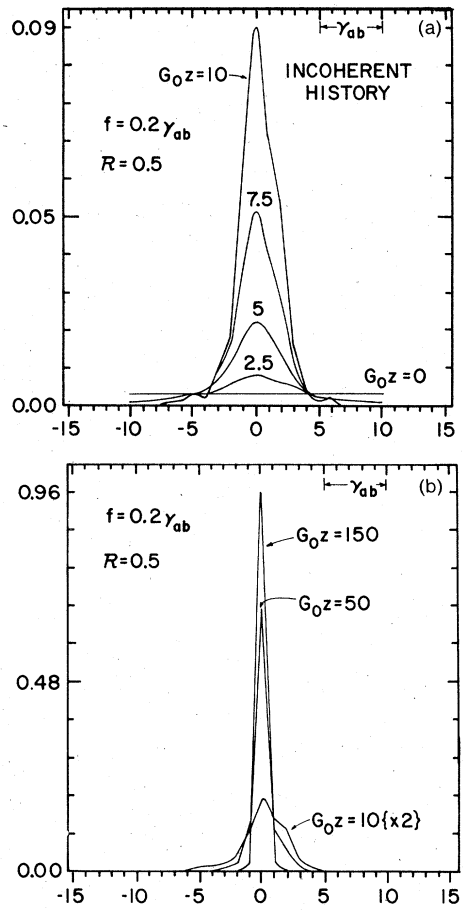

FIG. 1. Showing the spectral evolution of an incoherent history at increasing depths ($G_o z$) into the active medium. At $z=0$, the spectrum is flat $I_n(0)=2.5\times10^{-3}$, and phases $\phi_n(0)$ were randomly selected; numbers on the horizontal axis indicate detuning (nf) from the atomic frequency ω. Parameter values are: $f/\gamma_{ab}=0.2$, $\gamma_a=\gamma_b=\gamma_{ab}$, $\mathcal{R}=0.5$. Numerical integration of (2.28)–(2.30) with $\mathcal{W}(j)=\delta_{j,0}$. The spectrum tends toward the solution (4.2).

between $(-\pi,\pi)$. The ratio between the frequency interval and the different widths is $f/\gamma_{ab}=0.2$ ($\gamma_a=\gamma_b=\gamma_{ab}$); and the loss-gain ratio has the value $\mathcal{R}=\kappa/G_0=0.5$. For comparison, Figs. 2(a) and 2(b) show the spectral evolution undergone by a coherent history with the same initial spectrum. Parameter values are the same as in Figs. 1(a) and 1(b), but the initial phases are all taken to be zero. Since we are dealing with discrete spectra, the lines connecting the points in Figs. 1 and 2, do not have any physical meaning, and are drawn only for convenience; actually, the magnitude of the spectral intensities ought to be indicated by vertical lines drawn up from the zero base line. Finally, in conjunction with Figs. 1 and 2, Fig. 3 shows twice the power generation density,

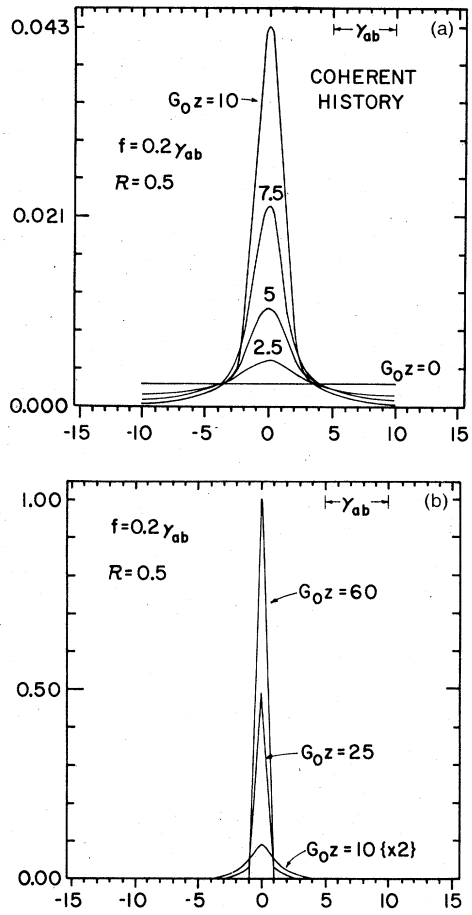

FIG. 2. Spectral evolution of a coherent history with the same initial spectrum as in Fig. 1(a), but the starting phases $\phi_n(0)$ were all taken to be zero. Parameter values in Figs. 2(a), 2(b) are those of Fig. 1. The spectrum tends toward the solution (4.2).

$$\tfrac{1}{2}\sum_n [\mathcal{E}_n^*(z)\rho_n(z)+\text{c.c.}], \tag{4.3a}$$

as a function of G_0z. This quantity acts as the source term in the evolution of the total intensity,

$$G_o^{-1}\frac{d}{dz}\sum_n I_n(z) = -\mathcal{R}\sum_n I_n(z) + \frac{1}{2}\sum_n [\mathcal{E}_n^*(z)\rho_n(z)+\text{c.c.}], \tag{4.3}$$

and from (2.19), we know that it is proportional to the time-averaged power density delivered to the field during $T=2\pi/f$. Because of the balance between atomic and field energy, this quantity also appears in the time-averaged population

$$D_o(z) = 1 - \tfrac{1}{2}\sum_n [\mathcal{E}_n^*(z)\rho_n(z)+\text{c.c.}]. \tag{4.4}$$

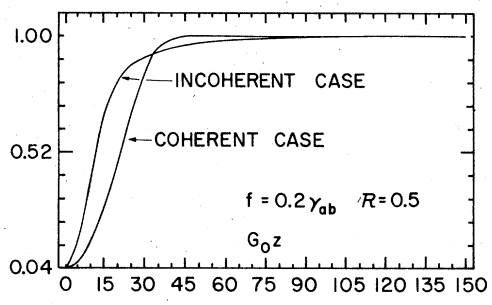

FIG. 3. Shows twice the power generation density (4.3a) vs distance (G_0z), for both the incoherent and coherent cases shown in Figs. 1 and 2, respectively. The curves show a different rate of saturation, with the same final value given by Eq. (4.2).

Figure 3 indicates that initially, the growth of the total intensity $[\sum_n I_n(z)]$ for the incoherent signal is faster than the corresponding growth for the coherent signal. In the present case, this is reasonable because the latter is a wave packet with an initial time duration, $\Delta\nu^{-1}\approx(0.25/\gamma)$ much shorter than the periodicity time $T=2\pi/f\approx 2\pi(5/\gamma)$. Correspondingly, at a given place z before the onset of saturation, the coherent signal extracts power from the atoms only during a small time $\Delta\tau \ll T$, and most of the energy pumped into the medium at a rate Λ (Eq. 2.2) during the interval $T>1/\gamma$ is lost by radiative decay. On the other hand, the incoherent signal with the same initial spectrum, but random phases, is an erratic function within the time interval T. The interaction with the atomic medium is less dramatic; however, the atomic energy pumped during T is continuously extracted by the field. The difference in the saturation rate between coherent and incoherent signals is enhanced in Fig. 4. There, the parameter values are

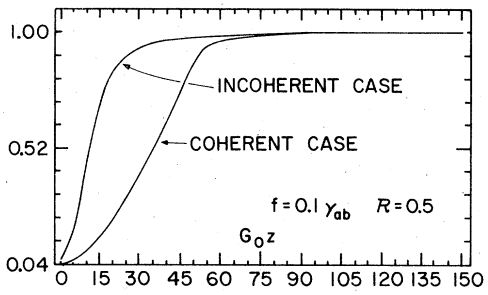

FIG. 4. Twice the power generation density (4.3a) vs distance (G_0z), for both coherent [$\phi_n(0)$'s = 0] and incoherent [$\phi_n(0)$'s, random set] histories. Parameter values are the same as in Figs. 1–3, except for a halving of the frequency interval: $(f/\gamma_{ab})=0.1$, $\gamma_a=\gamma_b=\gamma_{ab}$, $\mathcal{R}=0.5$. Differences in the saturation rate are larger than those shown in Fig. 3; however, the final value is the same.

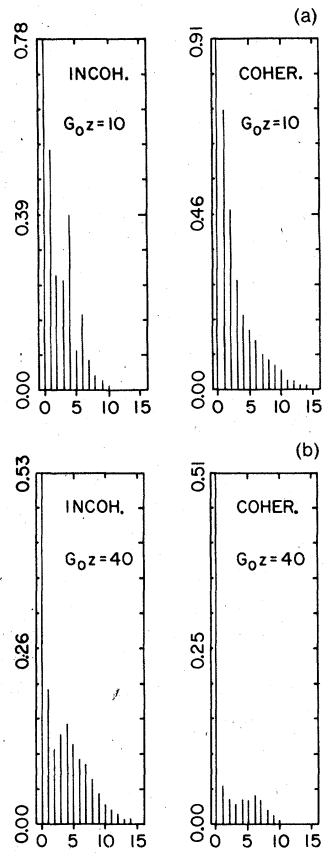

FIG. 5. Magnitude $|D_m(z)|$ of pulsations in the population—Eqs. (2.17), (2.30) with $\mathfrak{W}(j)=\delta_{j,0}$—for both the incoherent and coherent cases shown in Figs. 1 and 2. In Fig. 5(a), $G_0z=10$, while in Fig. 5(b) $G_0z=40$. For $m>0$, we have plotted $|D_m(z)|\times 10$. Interpretation of these results appear in the main text.

the same as in Figs. 1–3; but the period T has been doubled by diminishing the size of the frequency interval to $f/\gamma_{ab}=0.1$. Correspondingly, the number of "modes" has been doubled, and $I_n(0)=1.25\times10^{-3}$ for $|n|\leq 20$, and $I_n(0)=1.25\times10^{-5}$ for $20<|n|\leq 30$ (see Fig. 6). Comparing Fig. 4 with Fig. 3, we see that rate of growth for the incoherent signal has not changed much; however, the change is substantial for the coherent signal.

Figure 5(a) shows the magnitude $|D_m(z)|$ of pulsations in the population for both the incoherent and coherent cases at $G_0z=10$. Parameters are the same as those in Figs. 1 and 2 [note that for $m>0$, we have plotted $|D_m|\times 10$]. As expected, pulsations ($m\neq 0$) are smaller in the case where the phases are not correlated [see Eqs. (C11) and (C12)]. This is no longer true deep into the atomic medium because of the faster pace at which the sidebands disappear in the coherent pulse case, see Fig. 5(b) for $G_0z=40$. Indeed, a close inspection of Figs. 1 and 2 shows that the spectral narrowing rate is larger in the coherent case than in the case with uncorrelated phases. This can be explained because of the different saturation [e.g., $D_0(z)$] in both cases, as indicated by Figs. 3 and 4.

Spectral changes during propagation may be related to changes in the fraction $I_n(z)/I_0(z)$ of the line-center intensity at the frequency $\nu_n=nf$,

$$\frac{d}{dz}\frac{I_n(z)}{I_0(z)}=-\frac{I_n}{I_0}\left\{\frac{1}{I_0}\frac{dI_0}{dz}-\frac{1}{I_n}\frac{dI_n}{dz}\right\}. \tag{4.5}$$

From (2.28) with $\mathfrak{W}(j)=\delta_{j,0}$, we see that each term within curly brackets of (4.5) has the form

$$\frac{1}{I_n}\frac{dI_n}{dz}=-\kappa+\tfrac{1}{2}G_0\frac{1}{I_n}[\mathcal{E}_n^*(z)\rho_n(z)+\text{c.c.}], \tag{4.6}$$

and represents the "effective" gain coefficient at ν_n. At small signals, the effective gain depends mainly on detuning; however, as the signal grows, it also becomes a nonlinear function of the field through saturation (D_0) and mode-coupling effects (D_m). Substituting $\rho_n(z)$ given by (2.29) into Eq. (4.6), we can finally write (4.5) as

$$\frac{d}{dz}\frac{I_n(z)}{I_0(z)}=-\frac{I_n}{I_0}G_0\left[[1-\mathfrak{L}(n)]D_0(z)+\frac{1}{2}\frac{1}{I_0}\left(\sum_{m\neq 0}\mathcal{E}_0^*(z)\mathcal{E}_{-m}(z)D_m(z)+\text{c.c.}\right)\right.$$
$$\left.-\frac{1}{2}\frac{1}{I_n}\left(\mathfrak{D}(n)\sum_{m\neq 0}\mathcal{E}_0^*(z)\mathcal{E}_{n-m}(z)D_m(z)+\text{c.c.}\right)\right]. \tag{4.7}$$

In the present case, pulsations D_m are much smaller than D_0 (see Fig. 5). Therefore, the first line of (4.7) is sufficient to explain the different narrowing rates associated with the coherent and incoherent cases, $D_0(z)$ is larger in the coherent case [see Eqs. (C11) and (C12)]. As saturation sets in, $D_0(z)$ gradually diminishes from its starting value $D_0\approx 1$, toward its final value $D_0=\mathfrak{R}$, and the first line of (4.7) indicates the ensuing decrease of the narrowing rate. Finally, note that in the linear regime where $D_0\approx 1$ and $D_m\approx 0$, Eq. (4.7) gives

$$\frac{I_n(z)}{I_0(z)}\approx\frac{I_n(0)}{I_0(0)}\exp\left(-\frac{\nu_n^2}{\gamma_{ab}^2+\nu_n^2}G_0z\right). \tag{4.8a}$$

Since the ratio I_n/I_0 diminishes with distance, after a few steps into the active medium it is possible to define the spectral width as the separation be-

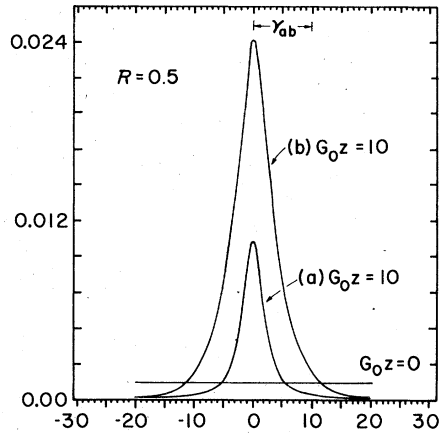

FIG. 6. Figures 6–9 compare different aspects of the narrowing process leading to single-mode oscillations [Eq. (4.2)], in two different cases, (a): $f = 0.1\ \gamma_{ab}$, $\gamma_a = \gamma_b = \gamma_{ab}$, and (b): $f = 0.1\ \gamma_{ab}$, $\gamma_a = \gamma_b = 0.1\gamma_{ab}$. In case (b), the population inversion density has a longer relaxation time. The loss-gain ratio is $\mathcal{R} = 0.5$; and the starting flat spectrum and phases are the same in both cases: $I_n(0)$'s $= 1.25\times10^{-3}$, $\phi_n(0)$'s $= 0$. Numerical integration of (2.28)–(2.30) indicate that the spectral evolution is more complex in case (b). Figure 6 shows the spectrum at $G_0z = 0$ and $G_0z = 10$.

tween the two frequencies for which $I_n(z)/I_0(z)$ is half its initial value. One readily obtains the known $z^{-1/2}$ dependence,[7,13,22]

$$\Delta\nu \approx \gamma_{ab}(\ln 2/G_0z)^{1/2} \quad \text{for } G_0z \gg \ln 2\,. \tag{4.8b}$$

In the case where γ_a ($\approx\gamma_b$) is much smaller than γ_{ab}, numerical integrations of (2.28)–(2.30) show that the spectral behavior (during the narrowing process that leads to single "mode" oscillations) is more complex than in the case where $\gamma_{ab} \approx \gamma_a$ ($\approx\gamma_b$). An example is shown in Figs. 6–9. In these plots, we compare the spectral evolution undergone by a low-level input signal in amplifiers with two different sets of parameters. In both cases, the loss-gain ratio is taken to be $\mathcal{R} = 0.5$, so that

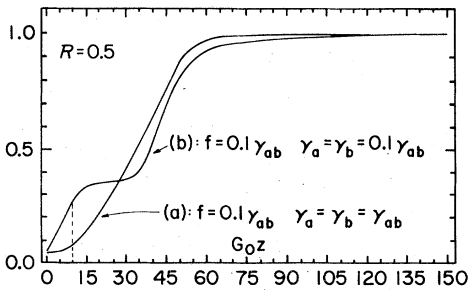

FIG. 7. Twice the power generation density (4.3a) vs amplifier depth G_0z, for cases (a) and (b) described in Fig. 6 and in main text.

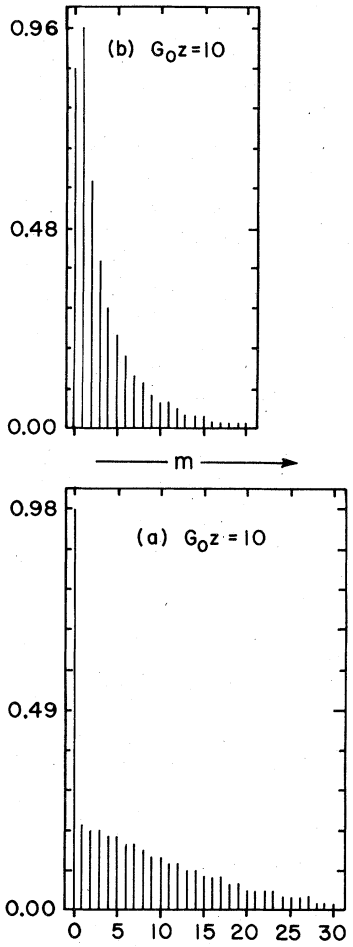

FIG. 8. Magnitude of population pulsations $|D_m(z)|$—Eqs. (2.17), (2.30) with $\mathcal{W}(j) = \delta_{j,0}$—for cases (a) and (b) described in Fig. 6. Pulsations are shown at $G_0z = 10$, still in the linear regime (see Fig. 7); and for $m > 0$ we have plotted $|D_m(z)| \times 10$.

the asymptotic value of the single mode solution is $I_0 = (1-\mathcal{R})/\mathcal{R} = 1$, whereas the linear passband [from $G_0\mathcal{L}(p) = \kappa$] is $\nu_p = \gamma_{ab}[(1-\mathcal{R})/\mathcal{R}]^{1/2} = \gamma_{ab}$. In one case we consider (a) $\gamma_{ab}/f = \gamma_a/f = \gamma_b/f = 10$, while in the other case we take a smaller breadth for the atomic levels (b) $\gamma_{ab}/f = 10$, $\gamma_a/f = \gamma_b/f = 1$.

The horizontal line in Fig. 6, represents the "flat" spectrum at the input; $I_n(0) = 1.25\times10^{-3}$ for $|n| < 20$, and $I_n(0) = 1.25\times10^{-5}$ for $|n| > 20$. The phases of the spectral components are all $\phi_n(0) = 0$. Thus, the input signal is a wave packet with a time duration $\Delta\tau \approx \frac{1}{4}\gamma^{-1}$, much smaller than the period $T = (2\pi/f)$. Frequencies, $\nu_n = nf$, are measured in units of f, and $n = 0$ stands for the atomic transition frequency ω. The spectrum for both cases, (a) and (b), at the distance $G_0z = 10$, is given by the lower and upper curves respectively. Figure 6 indicates that in the initial stages of the

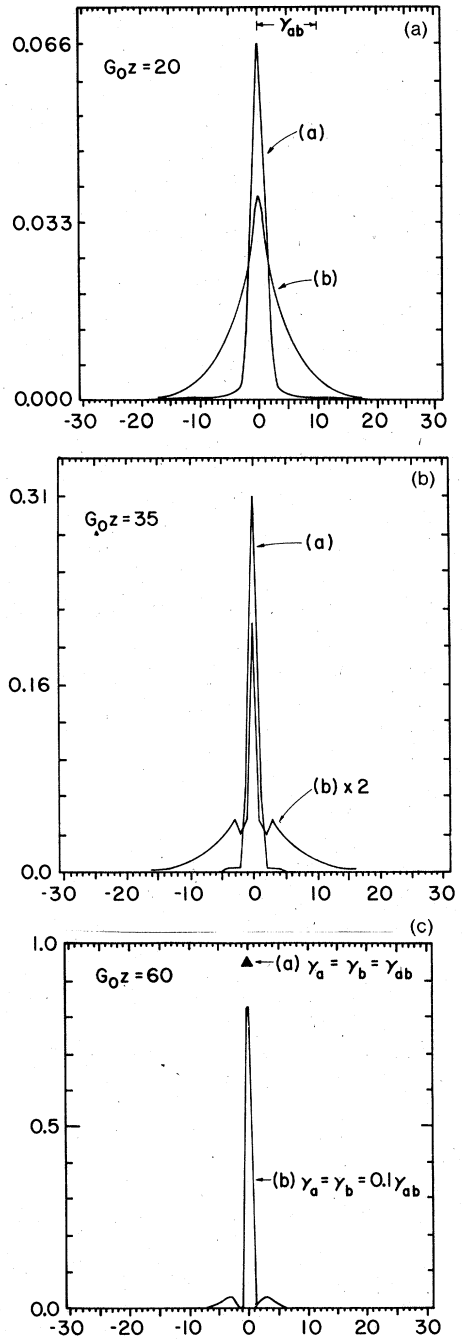

FIG. 9. Spectrum for cases (a) and (b) described in Fig. 6 is shown at different distances G_0z inside the amplifier.

amplification, the time-average power generation density [see Eqs. (4.3) and (4.4)] is higher in the case (b) than in (a); the population inversion density has a longer relaxation time in the former case, and the energy pumped into the medium is more efficiently extracted. Figure 7 shows (twice) the power generation density

$$\frac{1}{2}\sum_n [\mathcal{E}_n^*(z)\rho_n(z)] + \text{c.c.}$$

versus distances G_0z for both case (a) and (b).

Figure 7, in conjunction with Eq. (4.4) for the average population inversion, implies that, at least during the initial stages of the amplification,

$$D_0^{(a)} > D_0^{(b)};$$

and this is apparent in Fig. 8 showing the magnitude $|D_m(z)|$ of pulsations in the population for (a) and (b), at $G_0z = 10$. (Note that for $m > 0$, we have plotted $|D_m| \times 10$). From Fig. 8 one can see that $D_0^{(a)} \approx 0.98$, while $D_0^{(b)} \approx 0.86$; and this difference in conjunction with Eq. (4.7) partially explains the different narrowing rates associated with cases (a) and (b). Figures 9(a)–9(c) compare the spectrum at different distances inside the active medium. For convenience, the spectrum for case (b) has been multiplied by a factor of 2 in Fig. 9(b).

B. Monochromatic limit

The expressions (4.2) for quasimonochromatic oscillations are independent of the size of the frequency interval f; and in the numerical examples so far discussed in Sec. IV A, the interval was taken to be $f = 0.2\gamma_{ab}$ and $f = 0.1\gamma_{ab}$. We have also explored the "monochromatic limit" ($f = 0$) for quasimonochromatic oscillations at the atomic transition frequency ($\mathcal{E}_n = \mathcal{E}_0\delta_{n,0}$). For convenience, we started near the limiting value $|\mathcal{E}_0| = [(1 - \mathcal{R})/\mathcal{R}]^{1/2}$ subdivided among several components $\mathcal{E}_n$, and with increasingly smaller values for f. The rate at which the total intensity and power generation density of Eq. (4.3) grow toward their limiting values $(1 - \mathcal{R})/\mathcal{R}$ and $1 - \mathcal{R}$, do not change significantly. However, the narrowing process, i.e., the prevalence of the central mode over the side ones, slows down considerably by diminishing f because of the increasing coupling ($\propto \mathcal{F}(m)$) among the modes.[37] For small values: $f < 0.01\ \gamma_{ab}$, we were unable to observe appreciable narrowing beyond a spectral range $\Delta\nu \approx 0.05\gamma_{ab}$, in a reasonable amount of computer time.

The behavior described above, can be understood by taking a closer look at our basic equations in the monochromatic limit $f = 0$. In this case, the field amplitude (2.13) can be written

$$\mathcal{E}(z) = \sum_n \mathcal{E}_n(z). \tag{4.9}$$

However, the set $\{|\mathcal{E}_n|^2\}$ can no longer be interpreted as describing a spectrum since the $\{\mathcal{E}_n$'s$\}$ simply are complex vector components (phasors) with a resultant $\mathcal{E}$. Only $\mathcal{E}$ has a definite physical meaning as the field amplitude. The total intensity

will now be given by

$$I = \left(\sum_n \mathcal{E}_n\right)\left(\sum_k \mathcal{E}_k\right)^*,$$

which, in general, does not reduce to $\sum_n |\mathcal{E}_n|^2$. The individual components, $\mathcal{E}_n(z)$, still obey Eqs. (2.28)–(2.30), but now

$$\mathfrak{D}(n)|_{f=0} = 1, \quad \mathfrak{F}(m)|_{f=0} = 1, \tag{4.10}$$

for all n, m. Since we are interested in the evolution of the amplitude (4.9), instead of (2.28), we consider the sum

$$\partial_z \mathcal{E}(z) = -\tfrac{1}{2}\kappa \mathcal{E}(z) + \tfrac{1}{2}G_0 \sum_n \rho_n(z). \tag{4.11}$$

From (2.29) and (2.30) in conjunction with (4.10) we get

$$\sum_n \rho_n = \sum_n \sum_l \mathcal{E}_l D_{n-l}$$

$$= \sum_n \mathcal{E}_n - \tfrac{1}{2}\sum_n \sum_l \sum_q \mathcal{E}_l [\mathcal{E}_q^* \rho_{q+n-l} + \mathcal{E}_q \rho_{q-n+l}].$$

If the indices n, l, q, are unbounded, the above equation can be written in terms of the field amplitude (4.9) as

$$\sum_n \rho_n = \mathcal{E} - \tfrac{1}{2}\left(\mathcal{E}\mathcal{E}^* \sum_\mu \rho_\mu + \mathcal{E}\mathcal{E} \sum \rho_\mu^*\right);$$

and a similar expression for $\sum_n \rho_n^*$. From these equations, one obtains

$$\sum_n \rho_n = \frac{\mathcal{E}}{1 + \mathcal{E}\mathcal{E}^*},$$

which allow us to write (4.11) in the form

$$G_0^{-1}\partial_z \mathcal{E}(z) = \tfrac{1}{2}[\mathcal{E}/(1+I) - \mathcal{R}]. \tag{4.12}$$

Note that the steady state predicted by (4.12) agrees with (4.2). However, the individual components of $\mathcal{E} = \sum_n \mathcal{E}_n$, still evolve according to (2.28), and may or may not individually arrive to a steady state. As a matter of fact, numerical results indicate that they go on changing, but keeping a constant $\mathcal{E}$.[37]

C. Stability analysis.

We will now test the stability of the monochromatic solution by including with it small sidebands with complex spectral amplitudes ϵ_k, ϵ_{-k}, at each side of the steady state, $\mathcal{E}_0$, shown in (4.2). Then, the series (2.13) for the electric field amplitude reduces to

$$\mathcal{E}(z,t) = \mathcal{E}_0 + \epsilon_k(z) e^{-i\nu_k(t-z/c)} + \epsilon_{-k}(z) e^{+i\nu_k(t-z/c)}. \tag{4.13a}$$

If a sideband grows, the monochromatic solution $\mathcal{E}_0$ is unstable, and eventually a broader spectrum can develop. On the other hand, if all the sidebands decay, the narrow line solution is stable; although one cannot preclude the possibility of there being a stable broadband solution as well. Nevertheless, numerical computations with a range of different starting conditions did not provide any indication of this possibility.

Depending on the choice $\epsilon_{-k} = (\epsilon_k)^* = \epsilon e^{-i\phi}$, or $\epsilon_{-k} = -(\epsilon_k)^* = -\epsilon e^{-i\phi}$, the perturbation in (4.13) represents an amplitude modulation (AM),

$$\mathcal{E}(z,t) = \mathcal{E}_0 + 2\epsilon(z)\cos[\nu_k(t - z/c) - \phi(z)],$$

or a frequency modulation (FM),

$$\mathcal{E}(z,t) \approx \mathcal{E}_0 \exp\left(i\,\frac{2\epsilon(z)}{\mathcal{E}_0}\sin[\nu_k(t - 2/c) - \phi(z)]\right).$$

The gain for AM perturbations is always larger than for FM, and we will therefore consider only the first case.

We seek a solution of the coupled Eqs. (2.28)–(2.30) up to the first order in the small field amplitudes,

$$\mathcal{E}_n(z) = [\mathcal{E}_0\delta_{n,0} + \epsilon_k(z)\delta_{n,k} + \epsilon_{-k}(z)\delta_{n,-k}], \quad \epsilon_{-k} = \epsilon_k^*, \tag{4.13b}$$

$$\rho_n(z) = \rho_n^{(0)} + p_n(z), \quad D_m(z) = D_m^{(0)} + d_m(z). \tag{4.13c}$$

Substituting the above expressions into (2.28)–(2.30), we readily see that the zero-order terms are given by the steady-state values (4.2): $D_m^{(0)} = \mathcal{R}\delta_{m,0}$, $\rho_n^{(0)} = \mathcal{R}\mathcal{E}_0\delta_{n,0}$; and for the nonvanishing, first-order amplitudes we have the pair of equations

$$p_k = \mathfrak{D}(k)[\epsilon_k D_0^{(0)} + \mathcal{E}_0 d_k], \quad p_{-k} = p_k^*, \tag{4.14}$$

$$d_k = -\mathfrak{F}(k)[\mathcal{E}_0 p_k + \epsilon_k \rho_0^{(0)}], \quad d_{-k} = d_k^*. \tag{4.15}$$

We only need the explicit expression for

$$p_k = \mathfrak{D}(k)\epsilon_k D_0^{(0)}\left(\frac{1 - \mathfrak{F}(k)I_0}{1 + \mathfrak{F}(k)\mathfrak{D}(k)I_0}\right). \tag{4.16}$$

Note that the bracketed expression in (4.16) appears because of the second term in (4.14); i.e., because of population pulsation, while the first factor accounts for saturation effects.

A sideband will grow or decay depending on whether its net gain,

$$g_k = \frac{G_0^{-1}}{|\epsilon_k|^2}\,\frac{d|\epsilon_k|^2}{dz} = \left(-\mathcal{R} + \tfrac{1}{2}\,\frac{1}{|\epsilon_k|^2}[\epsilon_k^* p_k + \text{c.c.}]\right), \tag{4.17}$$

is positive or negative. Since

$$\mathcal{R} = \tfrac{1}{2}(1/I_0)(\mathcal{E}_0^*\rho_0^{(0)} + \text{c.c.}),$$

a simple inspection of (4.5)–(4.7), in conjunction

with (4.17), will show that instability $\mathcal{G}_k > 0$, if any, arises from pulsations in the population. Indeed, for moderate values of $\mathcal{R}$, the main contribution to p_k comes from the first term in (4.14) and in this case, the right-hand side of (4.17) is simply $-[1-\mathcal{L}(k)]D_0^{(0)} < 0$. This result is just the first term in (4.17), which is responsible for spectral narrowing. On the other hand, we shall see that for small values of $\mathcal{R} = \kappa/G_0$, the contribution of the second term of (4.14) can make (4.17) positive. In this case, the last two terms (4.7)—mode coupling due to pulsations—are able to overcome the spectral narrowing due to the first term.

Equation (4.16) and the definitions (2.31) and (2.32) for $\mathfrak{D}(k)$ and $\mathfrak{F}(k)$, allow us to write $\mathcal{G}_k$ explicitly in terms of $I_0 = (1-\mathcal{R})/\mathcal{R}$, the spectral location of the sidebands at each side of ω

$$\xi_k = \nu_k/\gamma_{ab}, \tag{4.18}$$

and the ratio

$$g = \gamma_a/\gamma_{ab} = \gamma_b/\gamma_{ab}, \quad 0 < g \leq 1. \tag{4.19}$$

After simple manipulations, the criterion for instability $\mathcal{G}_k > 0$, can be modified to read

$$-\xi_k^4 + \xi_k^2 g(3I_0 - g) - 2g^2(I_0^2 + I_0) > 0, \tag{4.20}$$

while less than zero, would mean that I_0 is a stable steady-state. The left-hand side of (4.20) has a maximum at each side of ω,

$$(\xi_k^2)_{\max} = \tfrac{1}{2} g(3I_0 - g).$$

The maximum value is positive (instability), for

$$\tfrac{1}{4}(3I_0 - g)^2 - 2(I_0^2 + I_0) > 0, \tag{4.21a}$$

i.e., instability occurs for

$$I_0 = \frac{1-\mathcal{R}}{\mathcal{R}} \geq (4+3g) + [(4+3g)^2 - g^2]^{1/2}. \tag{4.21b}$$

If (4.21b) is satisfied, then, sidebands will start to grow in the spectral range

$$|r_-| \leq |\xi_k| \leq |r_+|, \tag{4.22}$$

where $r_\pm$ are the roots of the polynomial (4.20),

$$r_\pm^2 = g\{\tfrac{1}{2}(3I_0 - g) \pm [\tfrac{1}{4}(3I_0 - g)^2 - 2(I_0^2 + I_0)]^{1/2}\}. \tag{4.23}$$

For example, if $g = 1$, the narrow line solution is unstable for intensity values $I_0 \geq 7 + 2\sqrt{12} \approx 13.93$, or equivalently, for loss-gain ratios $\mathcal{R} = (1+I_0)^{-1} \lesssim 0.07$; if $g \ll 1$, instability occurs for $I_0 \geq 8$ or $\mathcal{R} \lesssim 0.11$. Figure 10 shows the instability range (4.22)–(4.23) versus the intensity I_0 of the narrow line solution, for three different values of g: 1, 0.4, and 0.1. The upper and lower limits r_+, r_-, are indicated by the upper and lower branch on each curve. Numbers on the vertical axis measure frequencies in units of γ_{ab}. The figure also shows the value of the Rabi frequency ($\wp\,\mathcal{E}_0/\hbar\gamma_{ab}$).

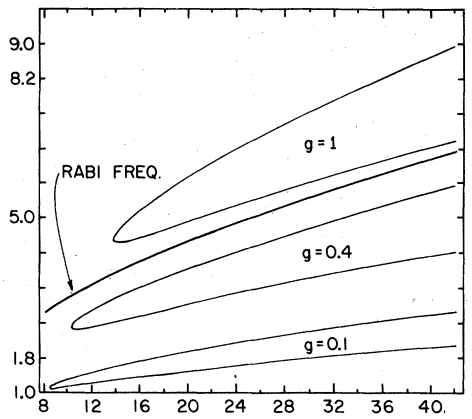

FIG. 10. Spectral range of instability of the narrow line solution (4.2). Frequencies are measured in units of γ_{ab} on the vertical axis, while numbers on the horizontal axis stand for the intensity of the narrow line solution $I_0 = (1-R)/R$. The upper and lower frequencies r_+, r_- of the instability range, (4.22), (4.23), are indicated by the upper and lower branch on each curve. The values of $g = \gamma_a/\gamma_{ab} = \gamma_b/\gamma_{ab}$ associated with the three curves, starting with the upper one: $g = 1$, $g = 0.4$, $g = 0.1$. The figure also shows the Rabi frequency in units of γ_{ab} ($\wp\,\mathcal{E}_0/\hbar\gamma_{ab}$).

The relation (4.21b) which defines the threshold for instability, can be readily recognized as equivalent to Eq. (3.10) in an article by Risken and Nummedal,[16] which deals with self-pulsing in a ring-laser configuration with one allowed direction of propagation. In the ring laser, the field is periodic in space with the cavity length as the period, and if the single mode operation is unstable, the instability can only grow in time: real wave vector and complex frequency. In our case, the field is periodic in time and the instability can only grow in space: complex wave vector and real frequency. The similarities between both problems are obvious, and indicate the possibility of self-pulsing and *soliton* propagation in a long laser amplifier with a high degree of atomic inversion. This problem deserves attention and will be dealt with in a future publication. Finally, we would like to mention that the stability of the narrow line solution can also be easily discussed by using the time-domain picture represented by Eqs. (2.9)–(2.12).[13,22]

V. BROAD LINE OSCILLATIONS: DOPPLER-BROADENED MEDIUM

A. Stability analysis for the narrow line solution

In the case of Doppler (inhomogeneous) broadening, Eqs. (2.28)–(2.30) still admit a steady-state, narrow line solution. As in (4.2), the steady-

state solution is obtained from (2.28)–(2.30) by considering constant amplitude ($d/dz \equiv 0$), single mode oscillations at the resonant frequency,

$$[I_n = I_a \delta_{n,o}, \rho_n(j) = \rho_0(j)\delta_{n,o}, D_m(j) = D_0(j)\delta_{m,o}],$$

$$\frac{dI_0}{dz} = -\kappa I_0 + \tfrac{1}{2} G \sum_j [\mathcal{G}_0^* \rho_0(j) + \text{c.c.}] \equiv 0,$$

$$\rho_0(j) = \beta^{-1} \mathfrak{D}(-j) \mathcal{G}_0 D_0(j),$$

$$D_0(j) = \mathfrak{W}(j) - \tfrac{1}{2}\beta[\mathcal{G}_0^* \rho_0(j) + \text{c.c.}], \qquad (5.1a)$$

where $\mathfrak{W}(j)$, β, G, and $\mathfrak{D}(j)$ are defined by (2.22), (2.25), (2.26), and (2.31), respectively.

From the last two equations we readily obtain the steady-state dc population difference for atoms of velocity $Kv_j = jf$,

$$D_0(j) = \frac{\mathfrak{W}(j)}{1 + I_0 \mathfrak{L}(j)}. \qquad (5.1b)$$

By using (5.1b) in conjunction with (3.17) for $\mathfrak{L}(j)$, the condition for constant amplitude can be written as

$$\beta^{-1} \sum_j D_0(j)\mathfrak{L}(j) = \frac{\beta^{-1}}{1+I_0} \sum_j \mathfrak{W}(j) \frac{\gamma_{ab}^2 (1+I_0)}{\gamma_{ab}^2 (1+I_0) + (jf)^2} = \frac{\kappa}{G}. \qquad (5.2)$$

As in (4.1) we define the loss-gain ratio, and use the same symbol

$$\mathfrak{R} = (\kappa/G), \quad 0 < \mathfrak{R} < 1 \text{ (above threshold)}. \qquad (5.3)$$

However, the reader should note that $G = G_0 \beta$ [see Eqs. (2.25)–(2.26)]. Equation (5.2) allows the computation of I_0 in terms of parameters of the system, and can be readily solved by iterations: Fig. 11 shows I_0 vs $\mathfrak{R}$ for $Ku = 10\gamma_{ab}$ and $Ku = 50\gamma_{ab}$. Note that for a fixed $\mathfrak{R}$ (abscissa) different Ku values imply different degrees of inversion in the active medium ($\mathfrak{R} = \kappa/G_0\beta$). For this reason we also give the values $\beta = 0.159$ and $\beta = 0.035$ associated with $Ku = 10\gamma_{ab}$ and $Ku = 50\gamma_{ab}$, respectively.[38]

Contrary to what happens in the homogeneous broadening case, we shall see that the narrow line solution becomes unstable for quite small values of I_0. Indeed, because of atomic motion there are atoms with different Doppler transition frequencies: $\nu_j = \omega(1 \pm v_j/c)$. Depending on the value of Ku, a wide range of radiation field modes may be driven by these atoms. That is, besides the I_0 oscillations, noisy sidebands may start to grow. For moderate to large shift values, $Ku > \gamma_{ab}$ to $Ku \gg \gamma_{ab}$, the sidebands cannot be quenched by the I_0 oscillations, since the second-order "hole burning" effects of I_0 are effective only over a range $K\Delta v \sim \gamma_{ab}$.

The stability analysis can be done as in the homogeneous broadening case, Sec. IV. Again we

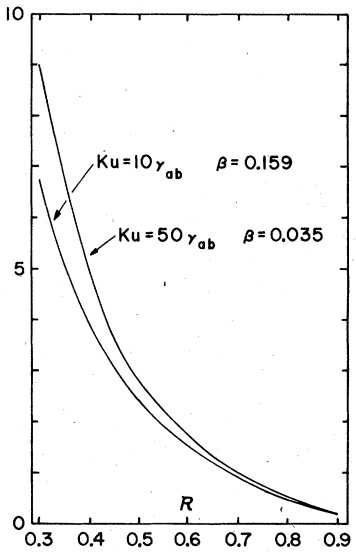

FIG. 11. Narrow line solution in Doppler-broadened media. The figure shows I_0 from Eq. (5.2), vs the loss-gain ratio (5.3) for two values of the Doppler width: $Ku = 10\gamma_{ab}$ and $Ku = 50\gamma_{ab}$. Reference 38 contains an expression for I_0 in the Doppler limit case.

include sidebands ϵ_k and ϵ_{-k} at each side of $\mathcal{G}_0$, Eq. (4.13b), and assume

$$\rho_n(z,j) = \rho_o^{(o)}(j)\delta_{n,o} + p_k(z,j)\delta_{n,k} + p_{-k}(z,j)\delta_{n,-k}, \qquad (5.4a)$$

$$D_m(z,j) = D_o^{(o)}(j)\delta_{m,o} + d_k(z,j)\delta_{m,k} + (d_{-k}(z,j)\delta_{m,-k}, \qquad (5.4b)$$

where

$$d_{-k}(z,j) = [d_k(z,j)]^*, \quad p_{-k}(z,j) = [p_k(z,-j)]^*. \qquad (5.4c)$$

We now seek a solution of (2.28)–(2.30) up to the first order in the small amplitudes. The zero-order terms are given by the steady-state values (5.1)–(5.2), and we need only the resultant expression

$$p_k(z,j) = \beta^{-1}\mathfrak{D}(k-j)\epsilon_k(z) D_0^{(o)}(j) \times \frac{1 - \tfrac{1}{2}\mathfrak{F}(k) I_0 \mathfrak{L}(j)}{1 + \tfrac{1}{2}\mathfrak{F}(k)[\mathfrak{D}(k-j) + \mathfrak{D}(k+j)] I_0}, \qquad (5.5)$$

which is a simple generalization of (4.16). As in (4.16), the bracketed expression in (5.5) appears because of population pulsations $d_{\pm k}$, while the first factor accounts for saturation effects. A sideband will grow or decay depending on whether its net gain,

$$\mathcal{G}_k = \frac{G^{-1}}{|\epsilon_k|^2} \frac{d|\epsilon_k|^2}{dz} = \left(\tfrac{1}{2} \frac{1}{|\epsilon_k|^2} \sum_j [\epsilon_k^*(z) p_k(z,j) + \text{c.c.}] - \mathfrak{R} \right), \qquad (5.6)$$

is positive or negative.

Figures 12(a) and 12(b) show $\mathcal{G}_k$ versus the spectral location of the sideband in units $f=\gamma_{ab}$ $(=\gamma_a,\gamma_b)$. The net gain is positive (instability) above the horizontal line and is negative below the line. In Fig. 12(a) $Ku=10\gamma_{ab}$ and $\beta\approx 0.159$, the lower curve represents the net gain when $I_0=0.1$ ($\mathfrak{R}\approx 0.95$), while the upper curve shows the gain when the resonant mode is $I_0=1$ ($\mathfrak{R}\approx 0.68$). In Fig. 12(b) the values of I_0 are the same as in Fig. 12(a) but $Ku=30\gamma_{ab}$ and $\beta\approx 0.057$.[38]

Contrary to the case of stationary atoms, in the present case, the values of $\mathfrak{R}$ needed for instability are much closer to threshold ($\mathfrak{R}=1$); also, mode-coupling effects are no longer essential in determining the instability of the narrow line solution. To show this we neglect the bracketed terms in (5.5), and consider only the first factor which contains saturation effects. Correspondingly, the right-hand side of (5.6) adopts a form which does not depend on population pulsations but only on saturation $D_0(j)$,

$$\mathcal{G}_k\approx\beta^{-1}\left(\sum_j \frac{\mathcal{W}(j)}{1+I_0L(j)}\,\mathcal{L}(k-j)-\mathfrak{R}\right). \tag{5.7}$$

The summation in (5.7) can be handled analytically if $\mathcal{W}(j)$ is much broader than $\mathcal{L}(j)$: $Ku\gg\gamma_{ab}$, "Doppler limit." In this case, the factor $\mathcal{L}(j)$ in the denominator clearly indicates that saturation effects are important only near the center of the line $\nu_k\lesssim\gamma_{ab}$. That is, the I_0 oscillations do not significantly deplete those atoms capable of feeding the sidebands, $Kv_j\approx\nu_k>\gamma_{ab}$. Then, the sidebands can grow nearly exponentially as long as the gain (first term in 5.7) is sufficient to overcome the losses. More explicitly, we express $\mathfrak{R}$ as the left-hand side of (5.2) and evaluate both terms of (5.7) in the Doppler limit approximation,[25]

$$\mathcal{G}_k\approx\beta^{-1}\left(\mathcal{W}(k)-\frac{\mathcal{W}(0)}{1+I_0}\right),\quad kf>\gamma_{ab},\quad Ku\gg\gamma_{ab}. \tag{5.8}$$

From (5.8) we can readily obtain a rough criterion for instability,

$$\exp[-(\nu_k/Ku)^2]>(1+I_0)^{-1}, \tag{5.9a}$$

and a gross estimate of the instability band

$$\gamma_{ab}<\nu_k<(Ku)[\ln(1+I_0)]^{1/2}. \tag{5.9b}$$

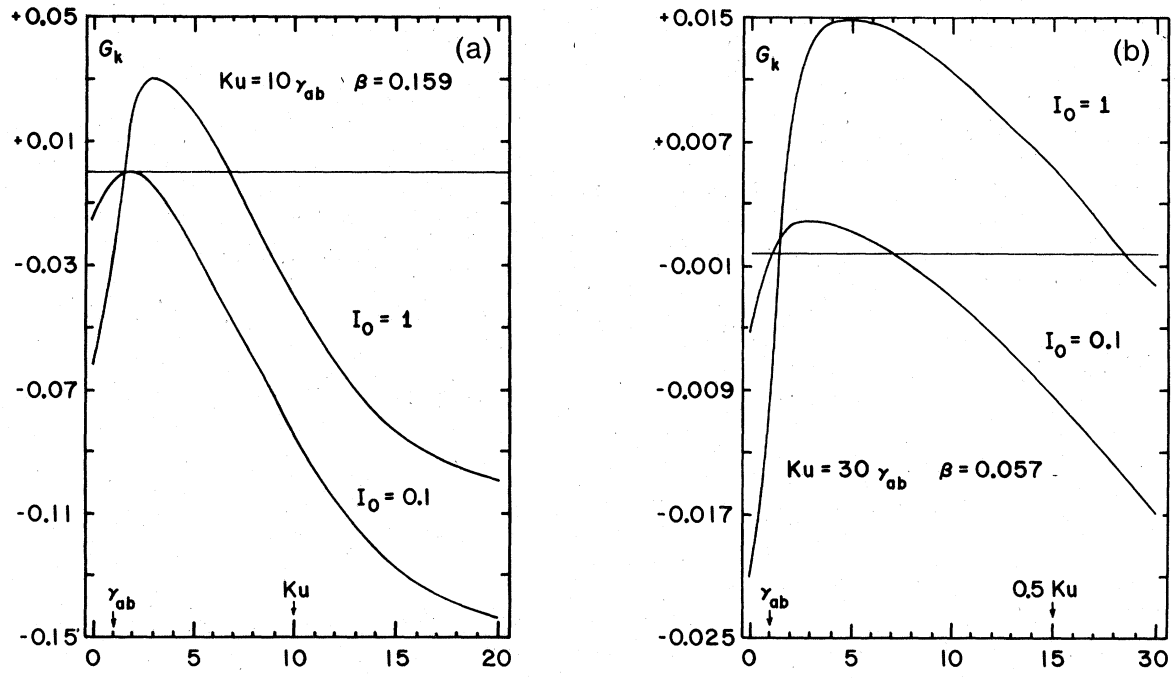

FIG. 12. Instability of the narrow line solution in Doppler-broadened media. Sideband noise will grow or decay depending on whether its net gain $\mathcal{G}_k$, Eq. (5.6), is positive or negative. The figures show $\mathcal{G}_k$ vs the location of the sideband (ν_k/γ_{ab}) in units of γ_{ab}, the net gain is positive (instability) above the horizontal line. In Fig. 12(a), $Ku=10\gamma_{ab}$, $\beta\approx 0.16$, the lower curve represents $\mathcal{G}_k$ when $I_0=0.1$, and in the upper curve $I_0=1$. In Fig. 12(b) the I_0 values are the same, but $Ku=30\gamma_{ab}$, $\beta\approx 0.06$.

Note that the right-hand side of (5.9b) and the linear passband

$$\nu_p = Ku[\ln(1/\mathcal{R})]^{1/2}, \tag{5.9c}$$

have, roughly, the same size.[38]

B. Spectral narrowing and rebroadening.

A number of experimental and theoretical articles have been published dealing with the spectral behavior of the radiation in nonlinear amplifiers.[5-9,22,27] In the course of amplification, the linewidth of the radiation first narrows, leading to some applications in spectroscopy.[39,40] In general, however, as the signal passes through enough gain medium to build near-saturation intensities, the linewidth of the radiation rebroadens again. Several theoretical articles on the subject are based on semiphenomenological, oversimplified rate equations and their treatment is inadequate. Hence, we wish to discuss indications given by our formalism which is based on first principles.

As in Sec. IV A, we will discuss changes in the fraction $I_n(z)/I_0(z)$ since they are directly related with spectral changes during propagation. For a generic member of the ensemble we have

$$\frac{d}{dz}\frac{I_n(z)}{I_0(z)} = -\left(\frac{I_n}{I_0}\right)\tfrac{1}{2}G\left(\frac{1}{I_0}\sum_j [\mathcal{E}_0^*\rho_0(z,j)+\text{c.c.}] - \frac{1}{I_n}\sum_j [\mathcal{E}_n^*\rho_n(z,j)+\text{c.c.}]\right). \tag{5.10}$$

By using (2.29) in the form

$$\rho_n(z,j) = \beta^{-1}\mathfrak{D}(n-j)\left(\mathcal{E}_n(z)D_0(z,j) + \sum_{\mu\pm 0}\mathcal{E}_{n-\mu}(z)D_\mu(z,j)\right), \tag{5.11}$$

Eq. (5.10) is written

$$\frac{d}{dz}\frac{I_n(z)}{I_0(z)} = -\frac{I_n}{I_0}G\beta^{-1}\left[\sum_j [\mathfrak{L}(j)-\mathfrak{L}(n-j)]D_0(j) + \tfrac{1}{2}\frac{1}{I_0}\sum_j\left(\mathfrak{D}(-j)\sum_{\mu\pm 0}\mathcal{E}_0^*\mathcal{E}_{-\mu}D_\mu(j)+\text{c.c.}\right) - \tfrac{1}{2}\frac{1}{I_n}\sum_j\left(\mathfrak{D}(n-j)\sum_{\mu\pm 0}\mathcal{E}_n^*\mathcal{E}_{n-\mu}D_\mu(j)+\text{c.c.}\right)\right], \tag{5.12}$$

with $\beta, G, \mathfrak{D}(j)$, and $\mathfrak{L}(j)$ defined by (2.25), (2.26), (2.31), and (3.17) respectively. Note that (5.12) is a generalization of (4.7), the first sum accounts for unsaturated gain differences and saturation effects, while the last two sums include mode-coupling phenomena.

In gas amplifiers with $Ku > \gamma_{ab}$, the effects of saturation are significantly different from those in homogeneously broadened amplifiers. In the inhomogeneous case, the onset of saturation not only decreases the gain-narrowing tendency, but may eventually produce rebroadening and restore the radiation to its Doppler line shape. This occurs because the center of the line saturates first, while the wings continue to grow nearly exponentially. For simplicity, let us start with a situation where pulsations do not contribute much [e.g., small coupling because of uncorrelated phases, see Appendix C, Eqs. (C11) and (C12)]. Then, $\rho_n(z,j)$ will be approximately given by the first term in (5.11) with

$$D_0(z,j) \approx \mathfrak{W}(j)\left(1+\sum_q I_q(z)\mathfrak{L}(q-j)\right)^{-1}, \tag{5.13}$$

and the transport equation for the spectral intensities adopts the explicit form

$$\frac{d}{dz}I_n(z) \approx I_n(z)\left(-\kappa + G\beta^{-1}\sum_j \frac{\mathfrak{W}(j)}{1+\sum_q I_q(z)\mathfrak{L}(q-j)}\mathfrak{L}(n-j)\right), \tag{5.14}$$

with $\mathfrak{W}(j)$ defined by (2.22).

We wish to determine for every depth z into the active medium, the sign and magnitude of (5.12) which is now approximately given by the first sum on right-hand side, i.e.,

$$\frac{d}{dz}\frac{I_n(z)}{I_0(z)} \approx -\frac{I_n}{I_0}G\beta^{-1}\sum_j [\mathfrak{L}(j)-\mathfrak{L}(n-j)]\frac{\mathfrak{W}(j)}{1+\sum_q I_q(z)\mathfrak{L}(q-j)}. \tag{5.15}$$

Analytical results are possible in the Doppler limit ($Ku \gg \gamma_{ab}$), and provided that the intensity spectrum remains broad compared with γ_{ab}. For example, we can write[25]

$$\sum_j \frac{\mathcal{W}(j)}{1+\sum_q I_q(z)\mathcal{L}(q-j)}\,\mathcal{L}(n-j) \approx \frac{\mathcal{W}(n)\sum_j \mathcal{L}(j)}{1+I_n(z)\sum_q \mathcal{L}(q)} = \frac{\mathcal{W}(n)[\beta/\mathcal{W}(0)]}{1+[\beta/\mathcal{W}(0)]I_n(z)}. \tag{5.16}$$

And Eqs. (5.14), (5.15) are given much simpler forms

$$\frac{d}{dz}J_n(z) \approx J_n(z)\left(-\kappa + G\,\frac{\exp[-(nf/Ku)^2]}{1+J_n(z)}\right) \tag{5.17}$$

$$\frac{d}{dz}\frac{J_n(z)}{J_0(z)} \approx -\frac{J_n}{J_0}\,G\left(\frac{1}{1+J_0(z)} - \frac{\exp[-nf/Ku)^2]}{1+J_n(z)}\right), \tag{5.18}$$

where,[25]

$$J_n(z) = [\beta/\mathcal{W}(0)]I_n(z) \tag{5.19a}$$

$$\approx [\pi\gamma_{ab}/f]I_n(z) = \pi\gamma_{ab}I(z,\nu_n) \quad \text{if } f \lesssim \gamma_{ab}. \tag{5.19b}$$

Equation (5.17) can be integrated in closed form, but we only need the saturation value

$$J_n(\infty) = \{\exp[-(nf/Ku)^2] - \mathcal{R}\}/\mathcal{R}, \tag{5.20}$$

where $\mathcal{R}$ is the loss-gain ratio (5.3). Expression (5.20) becomes negative for $nf > Ku[\ln(1/\mathcal{R})]^{1/2}$ and this is physically unacceptable. However, we shall see that numerical solutions of the exact coupled equations (2.28)-(2.30), closely approach a "truncated" version of (5.20) in situations where mode coupling does not contribute much compared with saturation effects ($|D_m| \ll |D_0|$).

Figure 13(a) shows $J_n(z)$ versus distance (Gz), both for $nf = 0$. and $nf = 0.5Ku$ (lower curve). The loss-gain ratio is $\mathcal{R} = 0.5$ and the Doppler limit has been assumed. The vertical lines indicate distances where the intensities attain half their saturation values $J_n(\infty)$. Figure 13(b) shows the sign and magnitude of the rate $(d/dz)[J_n(z)/J_0(z)]$ versus distance (Gz) as described by (5.18); as in Fig. 13(a), $\mathcal{R} = 0.5$ and $nf = 0.5Ku$. The horizontal line is the zero base line. Note that initially there is spectral gain narrowing; however, this process is reversed by the onset of saturation. Numerical results indicate that the inclusion of mode-coupling effects—last two terms on the right-hand side of (5.12)—do not change much the qualitative features shown in Fig. 13(a); but it can alter the rate of rebroadening as well as the spectrum, and in general should not be ignored. This is shown in Figs. 16(a), 19, 21, 23.

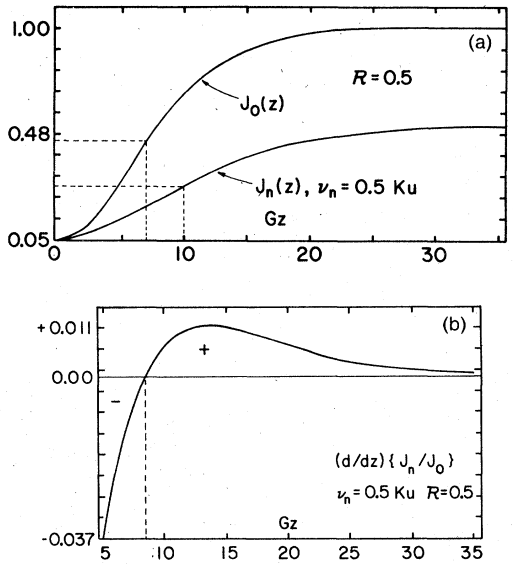

FIG. 13. Spectral narrowing and rebroadening in Doppler-broadened media. In this example, the effects of mode coupling are assumed to be small, and only saturation effects are considered. Figure 13(a) shows $J_n(z)$ vs Gz, both for $n = 0$ and $nf = 0.5\,Ku$ (lower curve), Eqs. (5.17)–(5.20). The loss-gain ratio is $\mathcal{R} = 0.5$, and the Doppler limit $Ku \gg \gamma_{ab}$ has been assumed. Figure 13(b) shows the sign and magnitude of $G^{-1}(d/dz)J_n(z)/J_0(z)$ vs Gz, Eq. (5.18). Note that the initial gain narrowing is reversed because $J_0(z)$ saturates before than $J_n(z)$.

C. Noise amplification in Doppler-broadened media: Numerical analysis

In this section we will describe and interpret numerical results obtained by computer integration of the set of Eqs. (2.28)–(2.30), applied to a few situations in Doppler-broadened active media. In each case, an "ensemble" of five different histories is built up, and for every member of the ensemble we applied the numerical method of Appendix C. The boundary condition at $z = 0$ was of low intensity, broad spectrum, and starting every time with a different set of randomly selected phases $\phi_n(0)$ with values between $(-\pi, \pi)$.

Because of the expense of performing the calculations, we have restricted ourselves to cases where the spectrum is symmetric around the atomic transition frequency $n = 0$,

$$\mathcal{E}_{-n}(z) = [\mathcal{E}_n(z)]^*, \quad \phi_{-n} = -\phi_n, \tag{5.21a}$$

which means that the field amplitude $\mathcal{E}(z,t)$, Eq. (2.13), is now taken to be real. This phase constraint represents, to some extent, a departure from a realistic representation of noise; nevertheless, the justification for its use is based on a comparison with a calculation in which the constraint is not used. Later, we shall see, at least in one case, that the effects of (5.21a) are easily

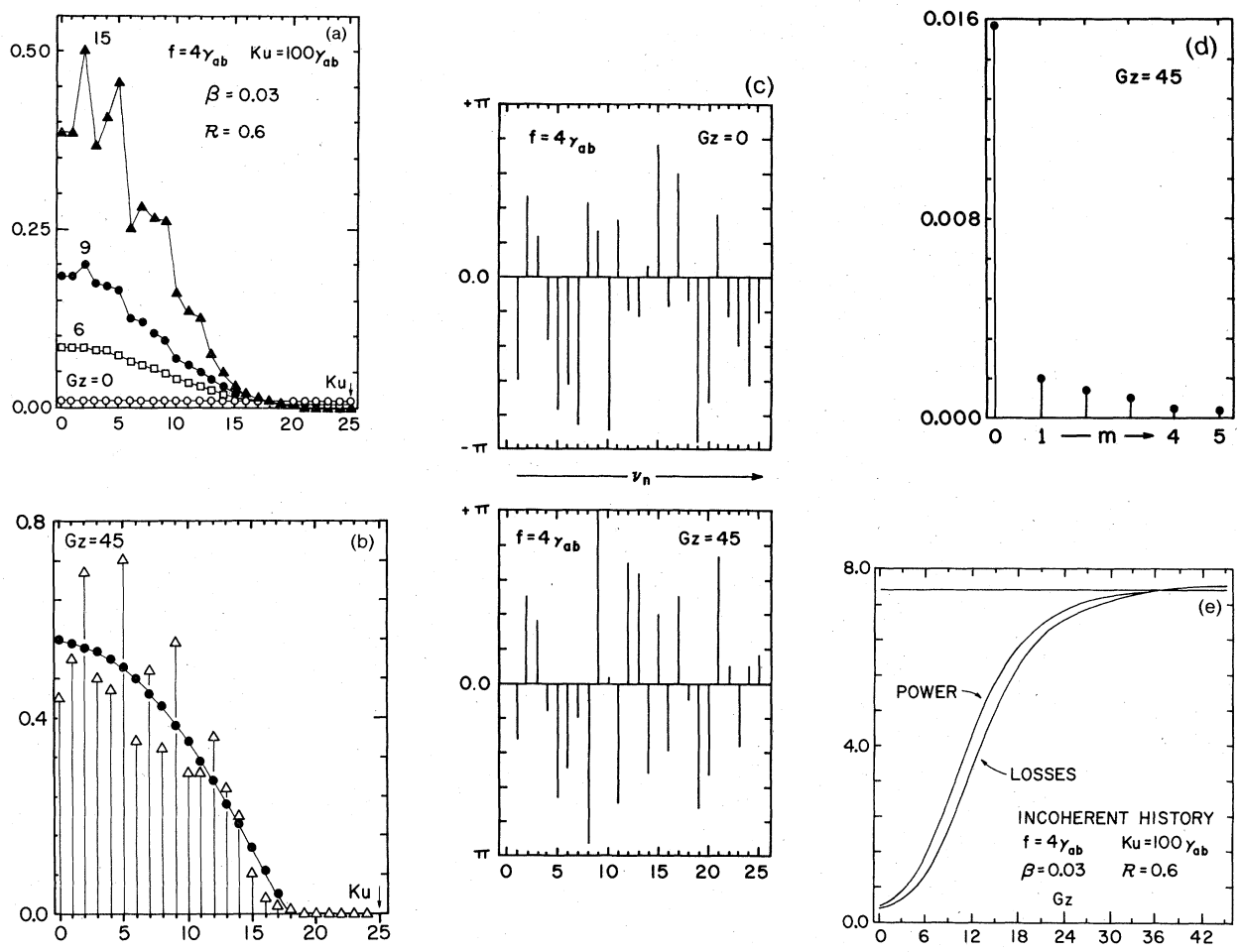

FIG. 14. (a) Evolution of an incoherent history in Doppler-broadened media, Eqs. (2.28)–(2.30), vs dimensionless distances Gz. With a large "mode separation" $f=4\gamma_{ab}$, and random phases $\phi_n(0)$ ($n>0$, $\phi_{-n}=-\phi_n$), mode-coupling effects are very small. A Doppler limit case $Ku=100\gamma_{ab}$, with $\mathfrak{A}=0.6$, $\gamma_a=\gamma_b=\gamma_{ab}$, and $\beta\approx 0.03$. The spectrum is symmetric around the atomic transition frequency and only one side is shown. The starting spectrum is flat $I_n(0)=0.01$ and extended over a frequency range $2Ku$. (b) The spectral intensities $I_n(z)$ in the saturation region $Gz=45$, see Fig. 14(e). The figure also includes the smooth spectrum obtained from (5.19a), (5.20) with parameter values given in Fig. 14(a). (c) Phases ϕ_n ($n>0$, $\phi_{-n}=-\phi_n$) of the incoherent history at $Gz=0$ and $Gz=45$. At $z=0$ the phases are selected with a random-number generator. (d) Shows $|D_m(z,j=0)|$ vs m for $Gz=45$, one can see that $D_0 >> |D_m|$, i.e., mode coupling effects contribute little. (e) The evolution of the total power generation density and losses vs Gz. The horizontal line indicates the saturation limiting value $\mathfrak{A}\sum_n I_n(\infty)\approx 7.6$ obtained from (5.19a) and (5.20) with parameter values given in Fig. 14(a).

understood. If one uses (5.21a) together with Eq. (2.18) ($D_{-m}=D_m^*$) then, the set of coupled equations (2.28)–(2.30) allow us to show that

$$D_m(z,j)=D_m(z,-j)\,, \tag{5.21b}$$

$$\rho_n(z,j)=[\rho_{-n}(z,-j)]^* \tag{5.21c}$$

where we have also taken into account that $\mathfrak{W}(j)=\mathfrak{W}(-j)$, Eq. (2.22). Furthermore, the relations (5.21) are maintained during propagation, i.e., they are constant of the motion of Eqs. (2.28)–(2.30).

In the first case we consider an extreme Doppler-limit case $Ku=100\gamma_{ab}$; and with little mode coupling compared with saturation effects, $|D_m| \ll D_0$. Equations (C11) and (C12) show that this can be achieved by starting with random phases $\phi_n(0)$ (for $n>0$, and $\phi_{-n}=-\phi_n$), and by taking a relatively large "mode separation" $f>\gamma$. Figures 14(a) to 14(e) show the evolution undergone by one particular history. Distances are measured in dimensionless units Gz, and frequencies in units of

$f=4\gamma_{ab}$. The atomic inversion is measured in terms of the loss-gain ratio $\mathcal{R}=0.6$; and for simplicity we have considered $\gamma_a=\gamma_b=\gamma_{ab}$. Given γ_{ab}, f and Ku, the resultant β, Eq. (2.25a), is $\beta \approx 0.028$.[25] Since the spectrum is the same at both sides of the atomic transition frequency, only one side is shown in the figures.

The initial spectrum at $Gz=0$, Fig. 14(a) is taken to be "flat", $I_n(0)=0.01$ for all n's, and extended over a frequency range of $2Ku$, while the starting phases [Fig. 14(c)], are selected with a random-number generator. Figure 14(a) shows the initial narrowing tendency, and also shows the start of the rebroadening process around $Gz=15$, where the nonlinear saturation regime appears to start [see Fig. 14(e)]. In Fig. 14(b) the vertical lines drawn up from the zero base line indicate the magnitude of the spectral intensities $I_n(z)$, in the saturation region $Gz=45$. This plot also includes the results obtained from expressions (5.19a) and (5.20) with the same parameter values. These expressions apply in the Doppler limit, and in a case where only saturation effects are important, which up to a certain extent, is the situation in our numerical example. Indeed, Fig. 14(d) shows $|D_m(z,j=0)|$ versus m for $Gz=45$, and from the graph one can see that $D_0 \gg |D_m|$, i.e., mode-coupling effects contribute little. Later on, we shall see that the fluctuations of I_n around the "theoretical curve" in Fig. 14(b) will, to some extent, wash-out after an average over a few different histories. Finally, Fig. 14(e) discloses the evolution of the total power generation density [see Eq. (2.19)],

$$\frac{1}{2}\sum_n \left(\mathcal{E}_n^*(z)\sum_j \rho_n(z,j)+\text{c.c.}\right),$$

and losses

$$\mathcal{R}\sum_n I_n(z),$$

versus distance Gz. The horizontal line indicates the saturation limiting value $\mathcal{R}\sum_n I_n(\infty)\approx 7.55$ for the "independent modes" situation described by Eqs. (5.19a) and (5.20).

The results discussed, so far, in this section describe the behavior of a generic history. These calculations were repeated five times, each time starting with different initial conditions: essentially five different sets of random phases $\phi_n(0)$'s. The spectral characteristics of the different members of the "ensemble" are shown in Fig. 15(a). For reasons of economy, we stopped the numerical integrations at $Gz=30.$, since for this distance both power and losses were close enough to their saturation value, see Fig. 14(e). The last history in Fig. 15(a) corresponds to that one previously discussed with some detail in Figs. 14(a)–14(e). After averaging over the ensemble, we obtain the spectrum shown in Fig. 15(b). The smooth curve in Figs. 15(a, b) is the spectrum in the absence of mode coupling, already shown in Fig. 14(b).

In every one of the different histories, Fig. 15(a), there is a dip at the center of the spectrum. This dip appears because of some mode coupling introduced by the constraint (5.21a) among phases at both sides of the central frequency. The central mode is more affected than the side modes by this type of combination tone. It is convenient to show this with some detail. Since $|D_\mu| \ll D_0$, Eq. (2.29) may be conveniently written

$$\rho_n(z,j)=\beta^{-1}\mathfrak{D}(n-j)D_0(z,j)\times[\mathcal{E}_n+\mathcal{E}_{n-1}(D_1/D_0)+\mathcal{E}_{n+1}(D_{-1}/D_0)+\mathcal{E}_{n-2}(D_2/D_0)+\mathcal{E}_{n+2}(D_{-2}/D_0)+\cdots],$$

and only a few terms need to be taken into account. Substituting the first term of the above expression into (2.30), we obtain an approximation

$$\frac{D_\mu}{D_0}\approx -\tfrac{1}{2}\mathfrak{F}(\mu)\sum_q[\mathcal{E}_q^*\mathcal{E}_{q+\mu}\mathfrak{D}(q+\mu-j)+\mathcal{E}_q\mathcal{E}_{q-\mu}^*\mathfrak{D}^*(q-\mu-j)].$$

Now, we wish to compare the effects of typical mode-coupling terms on the power delivered at two different frequencies, say $\mathcal{E}_0^*\rho_0(z,j)+\text{c.c.}$ and $\mathcal{E}_1^*\rho_1(z,j)+\text{c.c.}$ Because of the overall factors $\mathfrak{D}(-j)$ and $\mathfrak{D}(1-j)$ in front of the expressions for ρ_0 and ρ_1, respectively, the leading terms of D_μ/D_0 for use in each case are ($\mu>0$)

$$(D_\mu/D_0)_{j=0}\approx -\tfrac{1}{2}\mathfrak{F}(\mu)[\mathcal{E}_{-\mu}^*\mathcal{E}_0+\mathcal{E}_\mu\mathcal{E}_0^*]+\cdots,$$

$$(D_\mu/D_0)_{j=1}\approx -\tfrac{1}{2}\mathfrak{F}(\mu)[\mathcal{E}_{1-\mu}^*\mathcal{E}_1+\mathcal{E}_{1+\mu}\mathcal{E}_1^*]+\cdots.$$

Substituting these terms into the above forms for $\rho_0(z,j)$ and $\rho_1(z,j)$ we obtain

$$\rho_0(z,j)\approx\beta^{-1}\mathfrak{D}(-j)D_0(z,j)\{\mathcal{E}_0-\tfrac{1}{2}[\mathfrak{F}(1)\mathcal{E}_{-1}(\mathcal{E}_{-1}^*\mathcal{E}_0+\mathcal{E}_1\mathcal{E}_0^*)+\mathfrak{F}(1)^*\mathcal{E}_1(\mathcal{E}_1^*\mathcal{E}_0+\mathcal{E}_{-1}\mathcal{E}_0^*)+\mathfrak{F}(2)\mathcal{E}_{-2}(\mathcal{E}_{-2}^*\mathcal{E}_0+\mathcal{E}_2\mathcal{E}_0^*)+\mathfrak{F}(2)^*\mathcal{E}_2(\mathcal{E}_2^*\mathcal{E}_0+\mathcal{E}_{-2}\mathcal{E}_0^*)+\cdots]\},\tag{5.22}$$

$$\rho_1(z,j)\approx\beta^{-1}\mathfrak{D}(1-j)D_0(z,j)\{\mathcal{E}_1-\tfrac{1}{2}[\mathfrak{F}(1)\mathcal{E}_0(\mathcal{E}_0^*\mathcal{E}_1+\mathcal{E}_2\mathcal{E}_1^*)+\mathfrak{F}(1)^*\mathcal{E}_2(\mathcal{E}_2^*\mathcal{E}_1+\mathcal{E}_0\mathcal{E}_1^*)+\mathfrak{F}(2)\mathcal{E}_{-1}(\mathcal{E}_{-1}^*\mathcal{E}_1+\mathcal{E}_3\mathcal{E}_1^*)+\mathfrak{F}(2)^*\mathcal{E}_3(\mathcal{E}_3^*\mathcal{E}_1+\mathcal{E}_{-1}\mathcal{E}_1^*)+\cdots]\}.\tag{5.23}$$

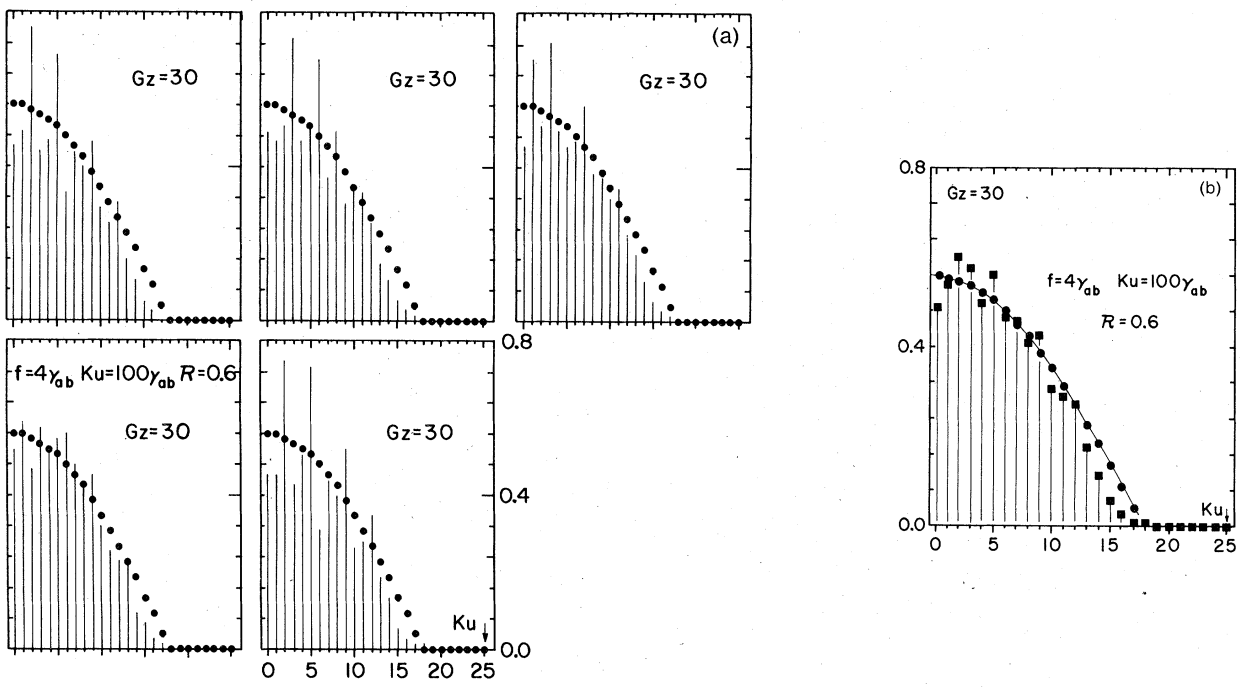

FIG. 15. (a) An "ensemble" of five different histories obtained with five different sets of starting random phases $\phi_n(0)$'s. The spectral intensities are shown at $Gz=30$. The last history in Fig. 15(a) corresponds to that one shown in Fig. 14. The smooth curve is the spectrum in the absence of mode coupling, already shown in Fig. 14(b). Parameter values are those of Fig. 14(a). (b) The figure shows the average over the "ensemble" shown in Fig. 15(a), and the smooth curve is the spectrum in the absence of mode coupling, Eqs. (5.19a), (5.20). They are indeed close; this shows that mode-coupling effects contribute very little in the present situation.

Depending on the degree of phase correlation, we may distinguish three cases.

(i) Uncorrelated phases: The first term in each parenthesis has a larger contribution than the second term, both in (5.22) and (5.23).

(ii) Uncorrelated phases with the constraint (5.21a): The first and second term in each parenthesis have the same contribution in the case of ρ_0; however, this is not so for ρ_1 because the second term has a smaller contribution. Correspondingly, the central mode is more affected by the extra mode-coupling effects, e.g., dip at the center of the spectrum.

(iii) Correlated phases: Dealing with pulse propagation, the contributions of both the first and second term in each parenthesis of (5.22) and (5.23) are nearly equal.

The strength of mode-coupling effects depend on the factors $\mathfrak{F}(m)$; then, dealing with noise, the spurious effects of the phase constraint (5.21a) are likely to increase by diminishing the size of the frequency interval f [see Eq. (2.32)].

In Fig. 16(a), we compare the spectrum obtained in three different situations, all of them at a distance close enough to saturation, $Gz=30$ [see also Fig. 16(c)]. The upper curve shows the analytical results (5.19a)–(5.20), which with the present parameter values ($Ku=100\gamma_{ab}$, $f=4\gamma_{ab}$, $\gamma_a=\gamma_b=\gamma_{ab}$, $\mathcal{R}=0.6$) is an approximate representation of the spectrum obtained by the ensemble average of the incoherent histories. The next curve represents a coherent pulse-propagation history, the initial spectrum was the same as in Fig. 14(a): $I_n(0)=0.01$ for all n's; however all the initial phases were taken to be $\phi_n(0)=0$. From the point of view of noise, this is a "pathological" history and was not taken into account in the ensemble shown in Fig. 15(a). Finally, the lower curve is the spectrum obtained from a numerical integration of the transport Eq. (2.33), where the power $\langle \mathcal{E}_n^*(z)\rho_n(z,j)\rangle$ was taken in the Litvak's approximation form, Eq. (3.11).[9]

Figure 16(b) shows the evolution undergone by the phases $\phi_n(z)$ of the coherent history. It is instructive to compare this figure with Fig. 14(c) for an incoherent history. Next, Fig. 16(c) compares the evolution of the total power generation density versus distance: (i) the upper curve represents the ensemble average of incoherent histories [see Fig. 15(a)], (ii) the curve in the middle

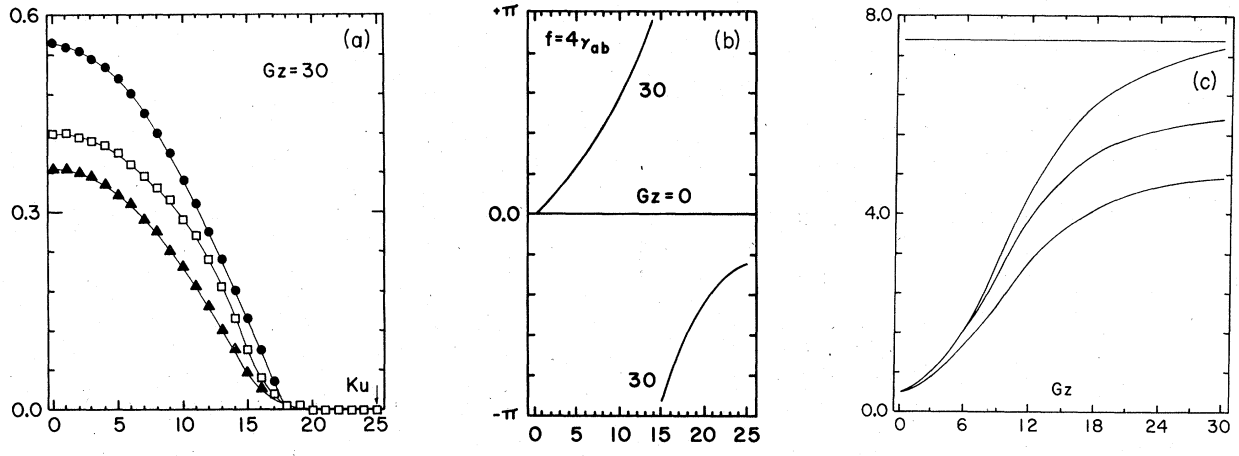

FIG. 16. (a) Shows the spectrum at $Gz=30$, for three different cases. The upper curve shows the analytical result (5.19)-(5.20), and is an approximate representation of the average shown in Fig. 15(b). The next curve represents a coherent-pulse history, the starting spectrum was the same as for the incoherent histories $I_n(0)=0.01$; however, the initial phases were all $\phi_n(0)$'s $=0$. The added phase correlation increases mode-coupling effects and the spectrum evolves differently. The lower curve is the spectrum obtained by numerical integration of (2.33), using Litvak's approximation (3.11). Parameter values are those of Fig. 14(a). (b) The evolution undergone by the phases $\phi_n(z)$ of the coherent history, Fig. 16(a). This figure should be compared with Fig. 14(c) which shows the evolution for an incoherent history. (c) Shows the total power generation density vs distance Gz. (i) The horizontal line indicates the saturation limiting value $\mathcal{R}\sum_n I_n(\infty)$, obtained from (5.19a), (5.20). (ii) The next curve is the resultant average over the ensemble of incoherent histories. (iii) The second curve represents the coherent history. (iv) The lower curve are results obtained using Litvak's approximation, Eq. (3.11).

represents the coherent history; and (iii) the lower curve shows similar results in the so called Litvak's approximation. Again, the horizontal line indicates the saturation-limiting value for the "independent modes" situation already shown in Fig. 14(e).

The difference between the saturation values associated with the incoherent and coherent signals can be explained by the same type of reasoning already used in Sec. IV. Namely, the wave packet has a time duration $\Delta\tau\approx(\mathrm{Ku})^{-1}=10^{-2}\gamma^{-1}$, which is much shorter than the period $T=2\pi/f\approx1.5\gamma^{-1}$. Correspondingly, the wave packet extracts power from the atoms only during a small time, and most of the energy continuously pumped into the medium during T is lost by radiative decay. On the other hand, the incoherent signal with similar spectrum, but random phases, is an erratic function in the time interval T, its interaction with the atoms is less dramatic, but the energy pumped during T is continuously extracted by the field. An alternative explanation takes into account the fact that pulsations D_m are larger, and D_0 is smaller in the coherent case, as compared with the same quantities for the incoherent signal.

Because of the considered range of parameter values, Figs. 15(a)–16(c), the results of the numerical integration of the transport Eq. (2.33) in conjunction with Litvak's approximation (3.11) can be discussed analytically. As we shall see, this procedure will clearly show that the main error of (3.11)—at least in this case—resides in the assumption of Gaussian statistics. Population pulsations do not contribute much in the situation at hand, and Eq. (3.11) may be approximated by

$$\langle\mathcal{E}_n^*(z)\rho_n(z,j)\rangle\approx\beta^{-1}\mathfrak{D}(n-j)\langle I_n(z)\rangle\left\{\mathfrak{W}(j)-\tfrac{1}{2}\beta\sum_q[\langle\mathcal{E}_q^*\rho_q\rangle+\langle\mathcal{E}_q\rho_q^*\rangle]-\tfrac{1}{2}\beta[\langle\mathcal{E}_n^*\rho_n\rangle+\langle\mathcal{E}_n\rho_n^*\rangle]\right\},\tag{5.24}$$

where the mode-coupling terms ($n\neq l$) have been left out. A simple inspection of the exact Eq. (3.10) in conjunction with its present form (5.24), show that the apparent "extra" terms in (5.24) originate in the factorization of fourth-order correlations, e.g.,

$$\langle\mathcal{E}_n^*\mathcal{E}_n\mathcal{E}_q^*\rho_q\rangle=(1+\delta_{n,q})\langle\mathcal{E}_n^*\mathcal{E}_n\rangle\langle\mathcal{E}_q^*\rho_q\rangle,$$

as approximately allowed by Gaussian statistics, see Eqs. (3.3) and (3.4).

From Eq. (5.24) we obtain the power density in terms of the intensities

$$\tfrac{1}{2}[\langle \mathcal{E}_n^*(z)\rho_n(z,j)\rangle + \text{c.c.}] = \beta^{-1}\mathcal{W}(j)\,\frac{\langle I_n\rangle}{1+\langle I_n\rangle}\,\mathfrak{L}^*(n-j)\Big/\Big(1+\sum_q \frac{\langle I_q\rangle}{1+\langle I_q\rangle}\,\mathfrak{L}^*(q-j)\Big)\,, \tag{5.25}$$

where $\mathfrak{L}^*$ has the same form as the Lorentzian (3.17) except for the modified width, $\gamma^* = \gamma_{ab}(1+\langle I_n\rangle)^{1/2}$. Using (5.25), the transport Eq. (2.33) is given the form

$$\frac{d}{dz}\langle I_n(z)\rangle \approx \langle I_n(z)\rangle\Big[-\kappa + G\beta^{-1}\,\frac{1}{1+\langle I_n\rangle} \times \sum_j \frac{\mathcal{W}(j)\,\mathfrak{L}^*(n-j)}{1+\sum_q \frac{\langle I_q\rangle}{1+\langle I_q\rangle}\,\mathfrak{L}^*(q-j)}\Big], \tag{5.26}$$

Eq. (5.26) is similar to (5.14) except for the saturation factor $(1+\langle I_n\rangle)^{-1}$, which originates in the "extra" terms of (5.24), that is, in the assumption of Gaussian statistics. We now consider the Doppler limit $Ku \gg \gamma^*$, and that the intensity spectrum remains broad compared with γ^* [these conditions are clearly satisfied by the numerical solution shown in Fig. 16(a)]. Hence, we can apply the procedure already used in (5.16) to obtain

$$\frac{d}{dz}\langle I_n\rangle \approx \langle I_n\rangle\Big(-\kappa + G\,\frac{\exp[-(nf/Ku)^2]}{(1+\langle I_n\rangle)^{1/2}+[\beta/\mathcal{W}(0)]\langle I_n\rangle}\Big). \tag{5.27}$$

The first term in the denominator departs from unity because of blackbody statistics. In the present case we can write $(1+\langle I_n\rangle)^{1/2} \approx 1+\frac{1}{2}\langle I_n\rangle$ [see Fig. 16(a)] and (5.27) can be given the same form as (5.17), but with a different scale factor. That is, instead of (5.19a) we now have

$$J_n = \{[\beta/\mathcal{W}(0)] + \tfrac{1}{2}\}\langle I_n\rangle\,. \tag{5.28}$$

Equation (5.28) together with (5.19a) indicate that numerical results shown in Figs. 16(a), 16(c)—which compare intensities $I^{(L)}$ obtained using Litvak's approximation [(2.33) and (3.11)], and those obtained from an ensemble average of histories obeying the exact [(2.28)–(2.30)]—should be approximately related by[25]

$$I_n^{(L)} \approx \{1+\tfrac{1}{2}[\mathcal{W}(0)/\beta]\}^{-1} I_n \approx \{1+\tfrac{1}{2}(\pi\gamma_{ab}/f)^{-1}\tanh(\pi\gamma_{ab}/f)\}^{-1} I_n\,. \tag{5.29}$$

With parameter values at hand, the first factor at the right-hand side of (5.29) is ≈ 0.7, which roughly agrees with the differences between the upper and lower curves in Figs. 16(a) and 16(c). The above relation does not hold for small values of f ($\lesssim \gamma_{ab}$), because mode-coupling effects are, then, important and have been neglected in the above derivation.

We consider, now, a second numerical example of noise amplification in Doppler-broadened media. The parameter values are taken to be: $\mathcal{R}=0.4$, $Ku = 25\gamma_{ab}$, $f=\gamma_{ab}$, $\gamma_a=\gamma_b=\gamma_{ab}$, with a resultant $\beta \approx 0.068$; as opposed to values used in the previous example: $\mathcal{R}=0.6$, $Ku=100\gamma_{ab}$, $f=4\gamma_{ab}$, $\beta\approx 0.028$. The spectrum at $Gz=0$, is again a low-intensity, "flat" spectrum, $I_n(0)=0.005$ for all n's; and every history starts with a different set of randomly selected phases (for $n>0$) with the phase constraint (5.21), $\phi_{-n}(0) = -\phi_n(0)$. In this example, the "smoothening" effects of Doppler shifts are diminished by taking a smaller Ku, and mode-coupling phenomena will have a larger contribution because of the smaller size of the frequency interval. For these reasons, one should expect large amplitude fluctuations, as well as some enhancement of the effects related with the constraint (5.21a). Indeed, we found that the central mode is, now, much more affected by the side modes, and in turn this effect further modifies mode coupling and saturation patterns. Correspondingly, the phase constraint (5.21a) ran counter to its intended purpose (saving computer expenses), since a larger number of histories are required to soften its spurious effects. This was not so obvious in the first numerical example of Fig. 15(a) since there, mode-coupling effects did not contribute much.

Figure 17 shows five different histories at Gz

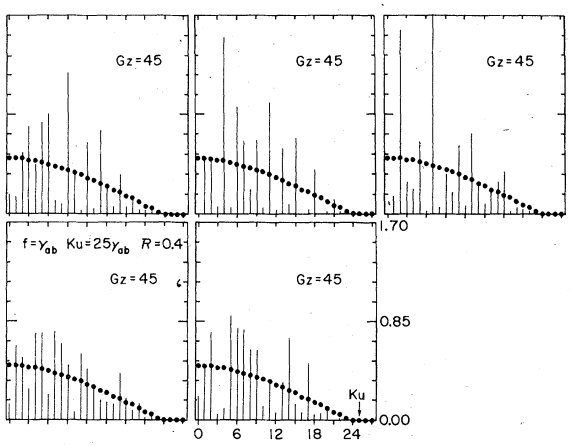

FIG. 17. A second numerical example of noise amplification in Doppler-broadened media, Eqs. (2.28)–(2.30). Parameter values are $\mathcal{R}=0.4$, $Ku=25\gamma_{ab}$, $f=\gamma_{ab}$, $\gamma_a=\gamma_b=\gamma_{ab}$, $\beta\approx 0.07$. The figure shows the spectrum for five different histories at $Gz=45$. At $z=0$ the spectrum is flat: $I_n(0)=0.05$ and every history starts with a different set of random phases $\phi_n(0)$ with the constraint (5.21a). Explanations in the main text. The smooth curves are obtained from (5.19) and (5.20).

=45, a distance well inside the saturation region (see Fig. 18). Fluctuations are quite large, and more so for those histories where the central mode has been more affected. The individual results appear useless, unless one is prepared to compute a large number of different histories. However, in spite of the vast differences among the members of the "ensemble", one can see from Fig. 18 that the evolution of the power density [also the losses $\mathcal{R}\sum_n I_n(\dot{z})$] versus distance is nearly the same for all of them; the small spread is depicted by the shaded area, while the solid curve stands for the ensemble average of the power density. The different histories also share a common spectral range, which appears to be nearly the same as the passband (5.9c),

$$\nu_p = Ku[\ln(1/\mathcal{R})]^{1/2}.$$

These characteristics will allow us to obtain useful qualitative information from our small ensemble, without further computer expenses.

The ensemble average is shown in Fig. 19 by the vertical lines drawn from the zero base line; and the lower curve depicts a spectrum described by expressions (5.19a) and (5.20); that is,

$$I_n = \frac{\mathcal{W}(0)}{\beta}\left(\frac{\exp[-(nf/Ku)^2]-\mathcal{R}}{\mathcal{R}}\right), \quad nf < \nu_p \tag{5.30}$$

with $\mathcal{W}(0) \approx \sqrt{\pi}(f/Ku) \approx 0.023$, $\beta \approx 0.068$. Let us recall that (5.30) apply in a case where mode coupling is negligible compared with the effects of saturation, and also $Ku \gg \gamma_{ab}$ was assumed. Our restricted ensemble does not allow a strict comparison between (5.30) and the ensemble average; this would require a larger ensemble to smooth the average. Nevertheless, a qualitative comparison is still possible since the spectral range ($\approx\nu_p$), and total intensity ($\sum\langle I_n\rangle \approx 6.34\mathcal{R}^{-1}$) are well defined at saturation distances (see Figs. 17 and 18). With this in mind, Fig. 19 shows the upper curve with the same functional form as (5.30); but instead of $\mathcal{W}(0)/\beta$ has a different amplitude A. The magnitude of $A(\approx 0.36)$ is determined by fitting the total intensity,

$$\sum_n \langle I_n\rangle \approx 2A\mathcal{R}^{-1}\int_0^{\nu_p}\{\exp[-(\nu/Ku)^2]-\mathcal{R}\}\,d\nu, \tag{5.31}$$

to the saturation value shown in Fig. 18. Since the lower curve in Fig. 19 does not take into account the effects of mode coupling, differences between this curve and the upper one, somehow provide a qualitative measure of these effects in the present situation. Figure 20 shows $|D_m(z,j)|$ versus m for $j=0$ at $Gz=45$. These magnitudes were obtained from the evolution of the last history shown in Fig. 17. The ratios $|D_m/D_0|$ should be compared with those associated with Fig. 14(d) belonging to the first

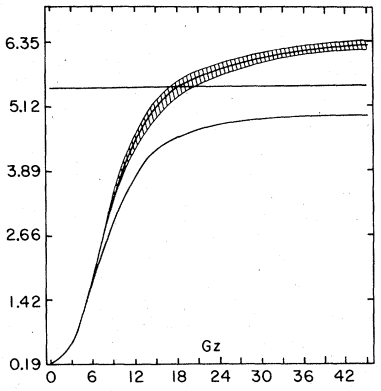

FIG. 18. Total power generation density vs distance Gz. The upper solid curve is the ensemble average. In spite of the vast spectral differences among members of the "ensemble," the power density is nearly the same for all histories. The small spread is depicted by the shaded area. The horizontal line represents the limiting saturation value, $\mathcal{R}\sum I_n(\infty)$, in the absence of mode coupling, Eqs. (5.19), (5.20). The lower curve is the power density one obtains using Litvak's approach (2.33) and (3.11).

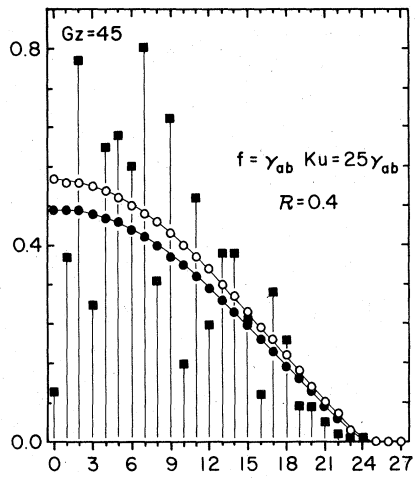

FIG. 19. Spectrum after average over the ensemble is depicted by the vertical lines. The lower curve is the spectrum in the absence of mode coupling, Eqs. (5.19) and (5.20). A strict comparison of this curve with the average is apparently not possible; this would require a larger ensemble to smooth the average. Since all histories have nearly the same spectral range and total intensity, $\sum_n I_n(z)$, a qualitative comparison is still possible. Indeed, the upper curve has the same functional form as the lower one, but its amplitude is determined by fitting the total intensity to the upper saturation value of Fig. 18. Differences are clearly due to mode-coupling effects.

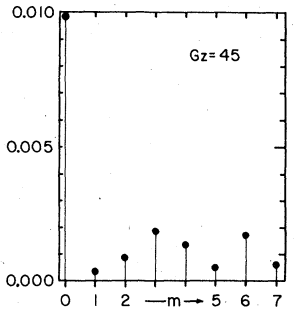

FIG. 20. Shows $|D_m(z,j)|$ vs m for $j=0$, at $Gz=45$. These magnitudes were obtained from the evolution of the last history shown in Fig. 17. The ratios $|D_m/D_0|$ should be compared with those associated with Fig. 14(d); one can see a significant increase in mode-coupling effects.

numerical example; one can see a significant increase in mode-coupling effects.

The curves shown in Fig. 19 appear again in Fig. 21 together with the lower curve which represents the spectrum obtained by numerical analysis of Eqs. (2.33) and (3.11) in the so-called Gaussian statistics approximation (i.e., Litvak's form). Similarly, the lower curve in Fig. 18 shows the evolution of the power generation density in the same approximation. Finally, Fig. 22 shows the phases associated with the last history in Fig. 17; i.e., $\phi_n(z)$ for $n>0$, at $Gz=0$ and $Gz=45$.

In the case at hand, the spectral behavior of the incoherent histories of Fig. 17, and the behavior of a coherent history having the same initial spectrum and $\phi_n(0)$'s $=0$, are quite different. Differences are larger than those shown in the first case, Fig. 16(a), because mode-coupling effects are now more important. Figures 23–27 show the evolution undergone by a coherent pulse during amplification. Parameter values are, again, those of Fig. 17; i.e., $\mathcal{R}=0.4$, $Ku=25\gamma_{ab}$, $f=\gamma_{ab}$, $\gamma_a=\gamma_b=\gamma_{ab}$, and $\beta\approx 0.068$.

Figure 23(a) shows the spectrum at successive distances inside the amplifier $Gz=0, 3, 6, 9, 12, 18$. Initially there is gain narrowing, and the rebroadening process starts between $Gz=9$ and $Gz=12$, at the onset of the saturation regime (see Fig. 24). Figure 23(b), shows the spectrum at $Gz=18$ and $Gz=45$, in the saturation region. While the passband for incoherent histories was approximately given by (5.9c), i.e., $\nu_p\approx 24\gamma_{ab}$; now, the spectral range is much larger ($>40\gamma_{ab}$). Spectral intensities and the total power generation density, Fig. 24, are substantially smaller than those shown in Fig. 21 and Fig. 18. The magnitude of pulsations in the population $|D_m(z,j=0)|$ at $Gz=45$, are depicted in Fig. 25. The values are approximately two times larger than those of Fig. 20 for an incoherent history. The phases $\phi_n(z)$ at $Gz=0, 6, 12, 18, 30, 45$, are shown in Fig. 26. Finally, a perspective view of the amplification undergone by the spectrum of the coherent history inside the amplifier, appears in Figs. 27(a) and 27(b).

ACKNOWLEDGMENTS

The authors are indebted to Dr. Frederic A. Hopf for interesting discussions, as well as for a

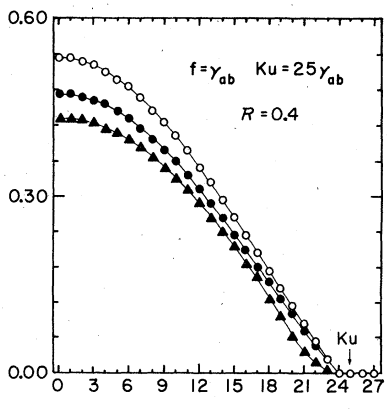

FIG. 21. Lower curve represents the spectrum obtained from (2.33) and (3.11) (Litvak's approximation.) The upper and middle curves are those already shown in Fig. 19.

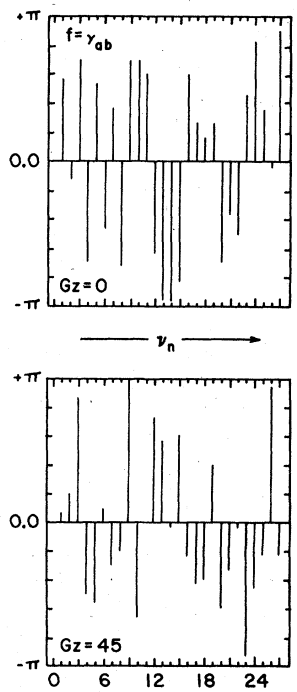

FIG. 22. Shows the phases associated with the last incoherent history in Fig. 17, i.e.: $\phi_n(z)$ for $n>0$, at $Gz=0$, and $Gz=45$.

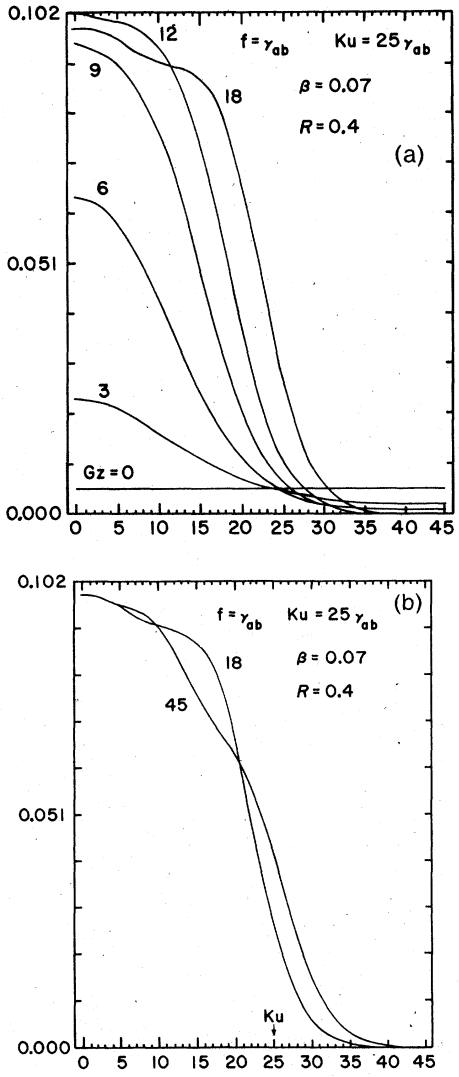

FIG. 23. (a) Shows the spectrum of a coherent history at successive distances inside the amplifier $Gz=0$, 3, 6, 9, 12, 18. Initially there is gain narrowing, and the rebroadening process starts at the onset of the saturation regime. Parameter values, and the spectrum at $z=0$ are the same as those of Fig. 17; but the starting phases are all zero, $\phi_n(0)$'s $=0$. (b) Same as Fig. 23(a) for $Gz=18$ and $Gz=45$, in the saturation region.

copy of his unpublished work on the subject. Also, we would like to thank Dr. Marvin M. Litvak for valuable comments and suggestions. This research was sponsored by the National Aeronautics and Space Administration, Grant No. NSG-5022, and the Air Force Office of Scientific Research.

APPENDIX A: FIELD-MEDIUM COUPLED EQUATIONS

It has been shown elsewhere,[2,3,15,19] that the equation of motion for $\underline{\rho}(z,t,v)$ and the field equation, can be written as

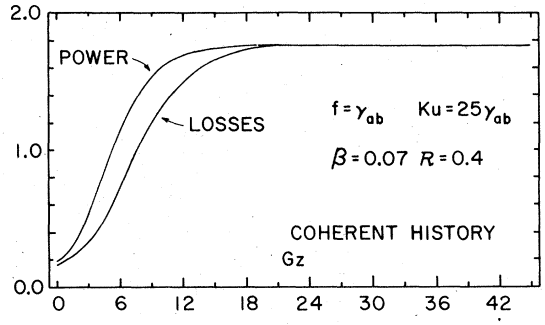

FIG. 24. Total power generation density, and losses $\Re\sum_n I_n$, vs distances Gz. Coherent history of Fig. 23.

$$\left(\frac{\partial^2}{\partial z^2}-c^{-2}\frac{\partial^2}{\partial t^2}-c^{-1}\kappa\frac{\partial}{\partial t}\right)E(z,t)=\mu_0\frac{\partial^2 P(z,t)}{\partial t^2}\ , \quad \text{(A1)}$$

$$\left(\frac{\partial}{\partial t}+v\frac{\partial}{\partial z}\right)\rho_{aa}(z,t,v)$$
$$=\lambda_a-\gamma_a\rho_{aa}-i(\wp/\hbar)E(z,t)(\rho_{ab}-\rho_{ba}), \quad \text{(A2)}$$

$$\left(\frac{\partial}{\partial t}+v\frac{\partial}{\partial z}\right)\rho_{bb}(z,t,v)$$
$$=\lambda_b-\gamma_b\rho_{bb}+i(\wp/\hbar)E(z,t)(\rho_{ab}-\rho_{ba}), \quad \text{(A3)}$$

$$\frac{\partial}{\partial t}+v\frac{\partial}{\partial z}\ \rho_{ab}(z,t,v)$$
$$=-(\gamma_{ab}+i\omega)\rho_{ab}-i(\wp/\hbar)E(z,t)(\rho_{aa}-\rho_{bb}), \quad \text{(A4)}$$

$$\rho_{ba}=\rho_{ab}^*, \quad \text{(A5)}$$

where $c=(\epsilon_0\mu_0)^{-1/2}$ is the velocity of light and

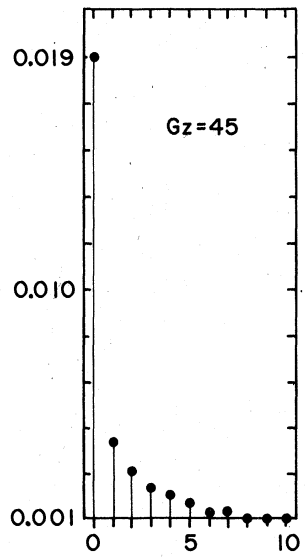

FIG. 25. Magnitude of pulsations in the population $|D_m(z,j=0)|$ at $z=0$ and $Gz=45$. Coherent history of Fig. 23.

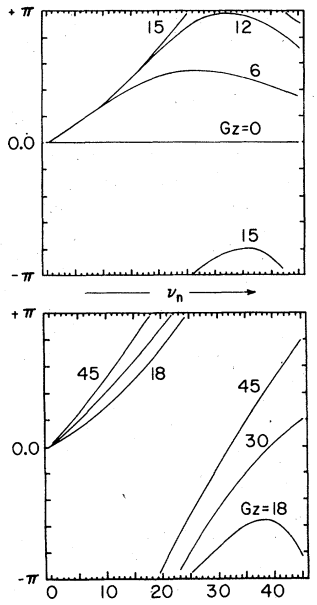

FIG. 26. Evolution undergone by the phases $\phi_n(z)$ of the coherent history, Fig. 23. Numbers on each curve stand for distances Gz.

$\omega = \omega_a - \omega_b > 0$ is the atomic transition frequency. The constant κ with dimensions of (length)$^{-1}$, is phenomenologically introduced as one simple way to deal with possible linear losses in the background medium. The damping constants $\gamma_a, \gamma_b \ll \omega$, and $\gamma_{ab} (> \frac{1}{2}(\gamma_a + \gamma_b)$, if collisions are taken into account), are introduced to represent the decay of levels a and b, and of the atomic dipole moment. The pumping rates, λ_a and λ_b are given by (2.2).

APPENDIX B: FIELD-MEDIUM EQUATIONS–FREQUENCY DOMAIN

Substituting the series (2.13) and (2.16)–(2.20) into Eqs. (2.9)–(2.12), one obtains the corresponding field-medium equations in the frequency domain. These equations couple only $\mathcal{E}_n(z)$ with $\rho_n(z, v)$ and $D_m(z, v)$,

$$\partial_z \mathcal{E}_n(z) = -\tfrac{1}{2}\kappa \mathcal{E}_n(z) + \frac{1}{2}\frac{\omega \wp}{c e_0}\int \rho_n(z, v)\, dv, \tag{B1}$$

$$\rho_n(z, v) = \frac{\wp}{\hbar}\left[\gamma_{ab} - i(\nu_n - \omega - Kv)\right]^{-1} \times \sum_l \mathcal{E}_l(z) D_{n-l}(z, v), \tag{B2}$$

$$D_m(z, v) = \left[(\Lambda_a/\gamma_a) - (\Lambda_b/\gamma_b)\right] W(v)\delta_{m,0} - \tfrac{1}{4}(\wp/\hbar)\left[(\gamma_a - i\nu_m)^{-1} + (\gamma_b - i\nu_m)^{-1}\right] \times \sum_q \left[\mathcal{E}_q^* \rho_{q+m} + \mathcal{E}_q \rho_{q-m}^*\right]. \tag{B3}$$

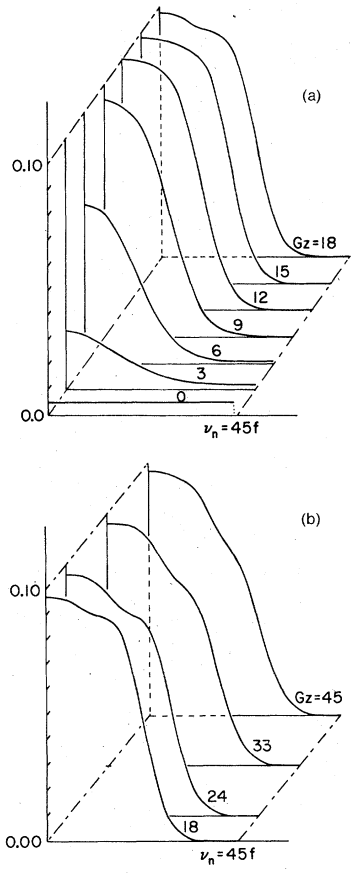

FIG. 27. A view of the amplification undergone by the spectrum of the coherent history (Fig. 23) inside the amplifier.

A transition to a continuous spectrum[23] is achieved by letting $\nu_n = nf \to \nu$, $f \to d\nu$, and $\mathcal{E}_n(z) \to \mathcal{E}(z, \nu)d\nu$, $\rho_n(z, v) \to \rho(z, \nu, v)d\nu$, $D_m(z, v) \to D_m(z, \nu, v)d\nu$, as well as $\delta_{m,0} \to \delta(\nu)d\nu$. The summations over l and q become integrals; e.g.,

$$\sum_l \to \mathcal{E}(\nu')D(\nu - \nu')\, d\nu',$$

and the spectral amplitudes $\mathcal{E}(z, \nu)$, $\rho(z, \nu, v)$, $D(z, \nu, v)$ will now have dimensions of $[\nu^{-1}]$, $[\nu^{-1}v^{-1}]$, $[\nu^{-1}v^{-1}]$, respectively. In the main test, these equations are given a more convenient, compact form by writing them out in terms of new dimensionless Fourier amplitudes.

APPENDIX C: A METHOD FOR NUMERICAL ANALYSIS OF EQS. (2.28)–(2.30)

The transport Eq. (2.28) for the field amplitudes may be dealt with by any of the well-known integration routines; e.g., "predictor-corrector" methods. For every z step into the active medium, it is necessary to compute the polarization

components $\rho_n(z,j)$ in terms of the set $\{\mathcal{E}_k$'s$\}$. Hence, we will concentrate on the pair of coupled Eqs., (2.29)–(2.30).

In actual computations, one considers a limited number of spectral components $\mathcal{E}_n$; say N of them on each side of the conventional origin ω: $-N,\ldots,-2,-1,0,1,2,\ldots,N$. Then, we have a total of $2N+1$ field "modes," and (2.29)-(2.30) may be given the explicit form

$$\rho_n(j)=\beta^{-1}\mathfrak{D}(n-j)\sum_{l=-N}^{l=+N}\mathcal{E}_l D_{n-l}(j)$$
$$=\beta^{-1}\mathfrak{D}(n-j)\sum_{\mu=n-N}^{\mu=n+N}\mathcal{E}_{n-\mu}D_\mu(j), \qquad \text{(C1)}$$

$$D_m(j)=\mathfrak{W}(j)\delta_{m,0}-\tfrac{1}{2}\beta\mathfrak{F}(m)\times\sum_{q=-N}^{q=N-m}[\mathcal{E}_q^*\rho_{q+m}(j)+\mathcal{E}_{q+m}\rho_q(j)^*], \qquad \text{(C2)}$$

where $0\le m\le 2N$, $D_{-m}=(D_m)^*$, and the z dependence is omitted. Note that we are also restricting the number of population pulsations D_μ: $-2N\le\mu\le+2N$.

Substituting (C1) into (C2) we get

$$D_m=\mathfrak{W}(j)\delta_{m,0}-\tfrac{1}{2}\mathfrak{F}(m)\sum_{q=-N}^{q=N-m}\Bigg(\sum_{\mu=q+m-N}^{\mu=q+m+N}\mathcal{E}_q^*\mathcal{E}_{q+m-\mu}\mathfrak{D}(q+m-j)D_\mu+\sum_{\mu=-q-N}^{\mu=-q+N}\mathcal{E}_{q+m}\mathcal{E}_{q+\mu}^*\mathfrak{D}^*(q-j)D_\mu\Bigg),\quad 0\le m\le 2N, \qquad \text{(C3)}$$

where for a fixed m, both μ sums have extreme upper and lower limits $\mu_U=+2N$, $\mu_L=-2N+m$. By inverting the order of the summations, Eq. (C3) can be written as[41]

$$D_m=\mathfrak{W}(j)\delta_{m,0}-\sum_{\mu=-2N+m}^{\mu=+2N}\mathfrak{A}_{m,\mu}D_\mu,\quad 0\le m\le+2N \qquad \text{(C4)}$$

with

$$\mathfrak{A}_{m,\mu}=\tfrac{1}{2}\mathfrak{F}(m)\Bigg(\sum_q{}^{\mathrm{I}}\,\mathcal{E}_q^*\mathcal{E}_{q+m-\mu}\mathfrak{D}(q+m-j)+\sum_q{}^{\mathrm{II}}\,\mathcal{E}_{q+\mu}^*\mathcal{E}_{q+m}\mathfrak{D}^*(q-j)\Bigg). \qquad \text{(C5)}$$

The extreme upper and lower limits for the (I) and (II) q sums in (C5) are indicated in Fig. 28. Depending on the value of the index μ, the matrix elements $\mathfrak{A}_{m,\mu}$ which enter in (C4) adopt the following explicit forms: For $\mu\le 0$:

$$\mathfrak{A}_{m,\mu}=\tfrac{1}{2}\mathfrak{F}(m)\sum_{q=-N}^{q=N-(m-\mu)}\mathcal{E}_q^*\mathcal{E}_{q+m-\mu}\times[\mathfrak{D}(q+m-j)+\mathfrak{D}^*(q-\mu-j)]. \qquad \text{(C6)}$$

For $\mu>0$, and $\mu<m$,

$$\mathfrak{A}_{m,\mu}=\tfrac{1}{2}\mathfrak{F}(m)\sum_{q=-N}^{q=N-m}[\mathcal{E}_q^*\mathcal{E}_{q+m-\mu}\mathfrak{D}(q+m-j)+\mathcal{E}_{q+\mu}^*\mathcal{E}_{q+m}\mathfrak{D}^*(q-j)]. \qquad \text{(C7)}$$

For $\mu>0$, and $\mu\ge m$,

$$\mathfrak{A}_{m,\mu}=\tfrac{1}{2}\mathfrak{F}(m)\sum_{q=-N}^{q=N-\mu}[\mathcal{E}_q\mathcal{E}_{q-q-m+\mu}^*\mathfrak{D}(q+\mu-j)+\mathcal{E}_{q+\mu}^*\mathcal{E}_{q+m}\mathfrak{D}^*(q-j)]. \qquad \text{(C8)}$$

The dependence of $\mathfrak{A}_{m,\mu}$ on the velocity index j, and coordinate z, is not shown explicitly.

Normally, it is convenient to extend the inferior limit of the sum (C4) from $\mu=-2N+m$ to $\mu=-2N$, this may be done by simply taking $\mathfrak{A}_{m,\mu}$

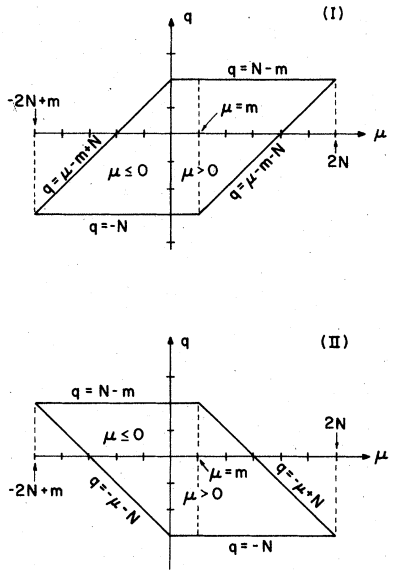

FIG. 28. The summation domain for sums $\sum^{\mathrm{I}}$ and $\sum^{\mathrm{II}}$ in Eqs. (C5) and (C4).

$\equiv 0$ for $\mu < -2N+m$. Up until now, we have only considered $m \geq 0$, the Eq. (C4) can be generalized to include the negative m values by noting that $D_{-|m|} = [D_{|m|}]^*$. This finally leads to

$$D_m = \mathfrak{W}(j)\delta_{m,0} - \sum_{\mu=-2N}^{\mu=+2N} \mathfrak{A}_{m,\mu} D_\mu, \quad -2N \leq m \leq 2N \tag{C9}$$

with

$$\mathfrak{A}_{-m,\mu} = [\mathfrak{A}_{m,-\mu}]^* \tag{C10}$$

and where the $\mathfrak{A}_{|m|,\mu}$ are given by (C6)–(C8), and $\mathfrak{A}_{|m|,\mu} \equiv 0$ if $\mu < -2N+m$.

Expression (C9) represents a set of $4N+1$ algebraic equations in the $4N+1$ pulsations for each j value: $\sum_\mu \mathfrak{M}_{m,\mu} D_\mu = \mathfrak{W}(j)\delta_{m,0}$, with $\mathfrak{M}_{m,\mu} = \delta_{m,0} + \mathfrak{A}_{m,\mu}$. In principle, the D_μ's may be obtained by matrix inversion methods; however, this is seldom necessary. For example, at small signals, $|D_0| \gg |D_\mu|$ with $\mu \pm 0$, and the second line of (C11) and (C12) which are shown below:

$$\begin{aligned} D_0(j) &= \frac{1}{1+\mathfrak{A}_{0,0}}\left(\mathfrak{W}(j) - 2\,\mathrm{Re}\sum_{\mu=1}^{2N} \mathfrak{A}_{0,\mu} D_\mu(j)\right) \\ &\approx \mathfrak{W}(j)[1+\mathfrak{A}_{00}]^{-1} \\ &= \mathfrak{W}(j)\left(1 + \sum_{q=-N}^{+N} \mathcal{E}_q^* \mathcal{E}_q \mathfrak{L}(q-j)\right)^{-1}, \end{aligned} \tag{C11}$$

$$\begin{aligned} D_m(j) &= -\frac{1}{1+\mathfrak{A}_{m,m}} \sum_{\mu(\pm m)} \mathfrak{A}_{m,\mu} D_\mu(j) \\ &\approx -[\mathfrak{A}_{m,0}/(1+\mathfrak{A}_{m,m})] D_0 \\ &= -\frac{\frac{1}{2}\mathfrak{F}(m) \sum_{q=-N}^{q=N-m} \mathcal{E}_q^* \mathcal{E}_{q+m} [\mathfrak{D}(q+m-j) + \mathfrak{D}^*(q-j)]}{1 + \frac{1}{2}\mathfrak{F}(m) \sum_{q=-N}^{q=N-m} [I_q \mathfrak{D}(q+m-j) + I_{q+m}\mathfrak{D}^*(q-j)]} D_0, \end{aligned} \tag{C12}$$

coincide with results that could be obtained by using perturbation theory. As the signal grows up, the D_μ's at $z+\Delta z$ can be obtained by iterations starting with the value of the D_μ's at z.

The approximations in (C11) and (C12) show that $|D_m| \ll |D_0|$ holds, not only at small signals $(\sum_q \mathcal{E}_q^* \mathcal{E}_q \mathfrak{L}(q-j) \ll 1)$; but also in the case where the spectrum is quasimonochromatic $(\Delta\nu < \gamma_a, \gamma_b)$, or there are several components separated by frequencies $|\nu_n - \nu_{n+1}| \gg \gamma_a, \gamma_b$. The expression (C12) also indicates that pulsations contribute significantly less if the phases are uncorrelated.

APPENDIX D: RANDOM, UNCORRELATED PHASES–STATIONARY STATISTICS

We now give arguments implying that if the phases of the radiation field are uncorrelated at some place z [e.g., see (3.6)], the response of the active medium is such that the phases will remain uncorrelated at $z+\Delta z$. The starting points are the field-medium coupled Eqs. (2.28)–(2.30),

$$\begin{aligned} \partial_z \mathcal{E}_n(z) &= -\tfrac{1}{2}\kappa \mathcal{E}_n(z) + \tfrac{1}{2}G \sum_j \rho_n(z,j), \\ \rho_k(z,j) &= \beta^{-1}\mathfrak{D}(n-j) \sum_l \mathcal{E}_l(z) D_{k-l}(z,j) \end{aligned} \tag{D1}$$

$$= \beta^{-1}\mathfrak{D}(n-j)\left(\mathfrak{W}(j)\mathcal{E}_k - \tfrac{1}{2}\beta \sum_l \sum_q \mathfrak{F}(k-l)\mathcal{E}_l [\mathcal{E}_q^* \rho_{q+k-l} + \mathcal{E}_q \rho_{q-k+l}^*]\right), \tag{D2}$$

and the assumption of random, uncorrelated phases at the place z,

$$\begin{aligned} &\langle \mathcal{E}_n^* \mathcal{E}_k \rangle_z = \langle I_n \rangle \delta_{n,k}, \\ &\langle \mathcal{E}_n^* \mathcal{E}_l \mathcal{E}_q^* \mathcal{E}_{q+k-l} \rangle_z = \ldots \delta_{n,k}, \\ &\langle \mathcal{E}_n^* \mathcal{E}_p \mathcal{E}_r^* \mathcal{E}_l \mathcal{E}_q^* \mathcal{E}_{q+r+k-p-l} \rangle_z = \cdots \delta_{n,k}, \\ &\qquad \cdots = \cdots. \end{aligned} \tag{D3}$$

The expression for ρ_k allow us to compute the polarization to any order in the field amplitudes, $\rho_k = \rho_k^{(1)} + \rho_k^{(3)} + \rho_k^{(5)} + \cdots$. This procedure is certainly valid at small signals, and sufficient for our plausible arguments. Using the iterative expansion of ρ_k in conjunction with relations (D3), one can see that

$$\begin{aligned} &\langle \mathcal{E}_n^* \rho_k \rangle_z = \langle \mathcal{E}_n^* \rho_n \rangle \delta_{n,k}, \\ &\langle \rho_n^* \rho_k \rangle_z = \langle |\rho_n|^2 \rangle \delta_{n,k}, \\ &\qquad \cdots = \cdots. \end{aligned} \tag{D4}$$

The relations (D4) imply that if the field is stationary, the response of the atomic medium is also stationary (see Ref. 31).

To compute $\langle \mathcal{E}_n^* \mathcal{E}_k \rangle_{z+\Delta z}$ for a small Δz into the medium we write

$$\langle \mathcal{E}_n^* \mathcal{E}_k \rangle_{z+\Delta z} = \langle \mathcal{E}_n^* \mathcal{E}_k \rangle_z + [\partial_z \langle \mathcal{E}_n^* \mathcal{E}_k \rangle]_z \Delta z + \tfrac{1}{2}[\partial_z^2 \langle \mathcal{E}_n^* \mathcal{E}_k \rangle]_z \Delta z^2 + \cdots, \tag{D5}$$

where the right-hand side can be evaluated with the help of the transport Eq. (D1). From (D1) one can show that

$$\partial_z \langle \mathcal{E}_n^* \mathcal{E}_k \rangle = -\kappa \langle \mathcal{E}_n^* \mathcal{E}_k \rangle + \tfrac{1}{2} G \sum_j [\langle \mathcal{E}_n^* \rho_k \rangle + \langle \mathcal{E}_k \rho_n^* \rangle],$$

$$\partial_z^2 \langle \mathcal{E}_n^* \mathcal{E}_k \rangle = -\kappa \partial_z \langle \mathcal{E}_n^* \mathcal{E}_k \rangle + \tfrac{1}{2} G \sum_j [\langle \partial_z \mathcal{E}_n^* \cdot \rho_k \rangle + \langle \mathcal{E}_n^* \cdot \partial_z \rho_k \rangle + \cdots],$$

and these equations, in conjunction with (D2), (D3), and (D4), imply that (D5) becomes

$$\langle \mathcal{E}_n^* \mathcal{E}_k \rangle_{z+\Delta z} = \langle I_n \rangle_{z+\Delta z} \delta_{n,k}. \tag{D6}$$

The arguments may now be repeated for a new slab, further into the atomic medium.

---

[1] W. E. Lamb, Jr., in *Lectures in Theoretical Physics*, edited by W. Brittin and B. Downs (Interscience, New York, 1960), Vol. II.

[2] A. Icsegvi and W. E. Lamb, Jr., Phys. Rev. 185, 517 (1969).

[3] F. A. Hopf and M. O. Scully, Phys. Rev. 179, 399 (1969).

[4] S. L. McCall and E. L. Hahn, Phys. Rev. 183, 457 (1969).

[5] L. Allen and G. I. Peters, Phys. Rev. A 8, 2031 (1973), with a list of related articles by the same authors.

[6] A. Yariv and R. Leite, J. Appl. Phys. 34, 3410 (1963).

[7] L. W. Casperson and A. Yariv, IEEE J. Quantum Electron. 8, 80 (1972).

[8] H. Maeda and A. Yariv, Phys. Lett. 43A, 383 (1973).

[9] M. M. Litvak, Phys. Rev. A 2, 2107 (1970).

[10] P. L. Bender, Phys. Rev. Lett. 18, 562 (1967).

[11] N. Evans *et al.*, Phys. Rev. A 6, 1646 (1972).

[12] P. Goldreich and J. Kwan, Astrophys. J. 190, 27 (1974), with a list of related articles by the same authors.

[13] M. Miller and A. Szöke, in Third Rochester Conference on Quantum Optics, June, 1972 (unpublished).

[14] See for example, W. E. Lamb, Jr., in *Quantum Optics and Electronics, Les Houches 1964,* edited by C. DeWitt, A. Blandin, and C. Cohen-Tannoudji (Gordon and Breach, New York, 1964), Lecture XV.

[15] See for example, M. Sargent, M. Scully, and W. Lamb, Jr., *Laser Physics* (Addison-Wesley, Reading, Mass., 1974), Ch. X.

[16] H. Risken, K. Nummedal, J. Appl. Phys. 39, 4662 (1968).

[17] H. Schlossberg and A. Javan, Phys. Rev. 150, 267 (1966).

[18] W. E. Lamb, Jr., Phys. Rev. 134, A1429 (1964).

[19] L. Menegozzi and W. E. Lamb, Jr., Phys. Rev. A 8, 2103 (1973).

[20] From Eq. (2.9), one can see that the energy conservation theorem takes the form

$$\partial_t \mathcal{U}(z,t) + \partial_z \mathcal{I}(z,t) = -\kappa \mathcal{I}(z,t) + (\tfrac{1}{4}\omega\wp) \times \int [\mathcal{E}^*(z,t)\rho(z,t,v) + \text{c.c.}]\, dv,$$

with

$$\mathcal{U}(z,t) = \tfrac{1}{2}\epsilon_0 |\mathcal{E}(z,t)|^2, \quad \mathcal{I}(z,t) = \tfrac{1}{2}\epsilon_0 c |\mathcal{E}(z,t)|^2.$$

The integrand represents the power per-unit-volume delivered to the radiation field by atoms of velocity v. This power has a familiar expression in terms of the overall field and polarization

$$(\tfrac{1}{4}\omega\wp)[\mathcal{E}^*(z,t)\rho(z,t,v) + \text{c.c.}] = -E(z,t)\dot{P}(z,t,v).$$

[21] N. Wax, *Selected Papers on Noise and Stochastic Processes* (Dover, New York, 1954), see especially S. O. Rice's article.

[22] F. Hopf, Optical Sciences Center, University of Arizona, "Noise Amplifiers" (unpublished).

[23] Formally, the transition to a continuous spectrum is readily accomplished with the following substitutions for (2.15), (2.14), and (2.13):

$$f = (2\pi/T) \to dv, \quad \nu_n = nf \to \nu,$$

$$\mathcal{E}_n(z) e^{i\nu_n z/c} = \frac{1}{T}\int_{-T/2}^{+T/2} [\mathcal{E}(z,t) e^{i(Kz-\omega t)}] \exp(i\nu_n t)\, dt \to \frac{d\nu}{2\pi}\int_{-\infty}^{+\infty} [\circ\circ\circ] \exp(i\nu t)\, dt = d\nu \mathcal{E}(z,\nu) e^{i(\nu z/c)},$$

$$\mathcal{E}(z,t) e^{i(Kz-\omega t)} = \sum_{n=-\infty}^{+\infty} [\mathcal{E}_n(z) \exp(i\nu_n z/c)] \exp(-i\nu_n t) \to \int_{-\infty}^{+\infty} d\nu [\mathcal{E}(z,\nu) e^{i(\nu z/c)}] e^{-i\nu t}.$$

[24] B. Fried and S. Conte, *The Plasma Dispersion Function* (Academic, New York, 1961).

[25] In the Doppler limit: $\eta = (\gamma_{ab}/Ku) \ll 1$; and in this case, the expression (2.25) admits a simple analytical form (see 2.22, $N_w \approx \pi^{\frac{1}{2}}$)

$$\beta = \sum_j \mathcal{W}(j)\mathcal{L}(j) \approx \mathcal{W}(0)\sum_j \frac{(\gamma_{ab}/f)^2}{(\gamma_{ab}/f)^2 + j^2} = \mathcal{W}(0) \times [(\pi\gamma_{ab}/f)/\tanh(\pi\gamma_{ab}/f)] = (\gamma_{ab}/Ku)\pi^{1/2}/\tanh(\pi\gamma_{ab}/f).$$

Note that for $f \lesssim \gamma_{ab}$ [already $\tanh(3) = 0.995$] above expression for β closely agrees with the more conventional one for the case of a continuum of atomic velocities.

$\beta = (\gamma_{ab}/Ku) Z_i(0, \gamma_{ab}/Ku) \approx (\gamma_{ab}/Ku)\pi^{1/2}$, for $\eta \ll 1$.

[26]The dimensionless intensity

$$I_n = [\wp^2 |\, \mathcal{E}_n\,|^2/\hbar^2\gamma\gamma_{ab}\,],$$

usually called saturation parameter, admits a simple interpretation in the case of weak, incoherent radiation at resonance with the transition $a \longleftrightarrow b$. In this case, I_n represents the ratio between the stimulated (R_s) and spontaneous (γ) emission rates. Indeed, if the frequency spread is of the order γ_{ab}, Fermi's golden rule gives

$$R_s = 2\pi\hbar^{-1}|\, H_{b/a}\,|^2\rho_f = 2\pi\hbar^{-1}|\tfrac{1}{2}\wp\,\mathcal{E}_{\overline{n}}|^2(1/\hbar\gamma_{ab}),$$

and

$$R_s/\gamma = \tfrac{1}{2}\pi I_{\overline{n}} \cdot$$

[27]J. H. Parks, *Esfahan Symposium on Fundamental and Applied Laser Physics*, edited by M. Feld, A. Javan, and N. Kurnit (Wiley-Interscience, New York, 1971), p. 867.

[28]L. Mandel and W. Wolf, Rev. Mod. Phys. 37, 231 (1965).

[29]R. Glauber, Phys. Rev. 131, 2766 (1966), see p. 2780.

[30]Strictly speaking, the distribution is Gaussian in terms of the random variables $\mathrm{Re}(\mathcal{E}_k)$ and $\mathrm{Im}(\mathcal{E}_k)$. The complex wave amplitude $\mathcal{E}(O,t)$ is a sum of Gaussian random variables.

[31]The relation (3.6) in conjunction with the series representation (2.13), indicates the "stationary" character of the statistics. That is, if the phases are not correlated; then, all ensemble averages are independent of the origin of time; e.g.,

$$\langle \mathcal{E}^*(0,t)\,\mathcal{E}(0,t+\tau)\rangle \propto \sum_n \langle I_n(0)\rangle \exp[-i(\nu_n - \omega)\tau].$$

[32]P. Goldreich *et al.*, Astrophys. J. 179, 111 (1973); see p. 113 and Appendix A.

[33]F. Hopf, 1974 IEEE International Quantum Electronics Conference Digest of Technical Papers, p. 41 (unpublished).

[34]The complex function $Z(\nu_n/Ku, \gamma_{ab}/Ku)$ is, in fact, a function of a single complex variable

$$\zeta = (\nu_n/Ku) + i(\gamma_{ab}/Ku),$$

and its derivative is given by (Ref. 24)

$$\frac{dZ(\zeta)}{d\zeta} = -2[1 + \zeta Z(\zeta)].$$

[35]H. Gamo, S. Chuang, paper presented at the Third Rochester Conference on Coherence and R. Optics, June, 1972 (unpublished).

[36]H. Gamo, H. Osada, paper presented at the Annual Meeting of the Optical Society of America, Tucson, Arizona, October, 1976 (unpublished).

[37]W. E. Lamb, Jr. and L. Menegozzi, 1974 IEEE International Quantum Electronics Conference Digest of Technical Papers, p. 41 (unpublished).

[38]Equation (5.2) shows that except for the modified width of the Lorentzian, $\gamma^* = \gamma_{ab}(1+I_0)^{1/2}$, the sum at the left-hand side is similar to the definition (2.25) for β. An explicit solution for I_0 can be obtained if $\gamma^* << Ku$, i.e., $n = (\gamma_{ab}/Ku) << 1$ and not too large values of I_0 (Ref. 25),

$$(1+I_0) \approx \frac{\pi}{[\mathfrak{R}(\sqrt{\pi} - 2n) + 2n]^2} \approx \mathfrak{R}^{-2} \cdot$$

[39]G. Birnbaum, Proc. IEEE 55, 1015 (1967).

[40]J. Parks, D. Ramachandra Rao, and A. Javan, Appl. Phys. Lett. 13, 142 (1968).

[41]J. Hambenne and M. Sargent III, Phys. Rev. A 13, 784 (1976).